A widely distributed gene cluster compensates for uricase loss in hominids

Liu, Yuanyuan; Jarman, Bryce; Low, Yen S.; Augustijn, Hannah E.; Huang, Steven et al

https://doi.org/10.1016/j.cell.2023.06.010

Cell

A widely distributed gene cluster compensates for uricase loss in hominids

Graphical abstract
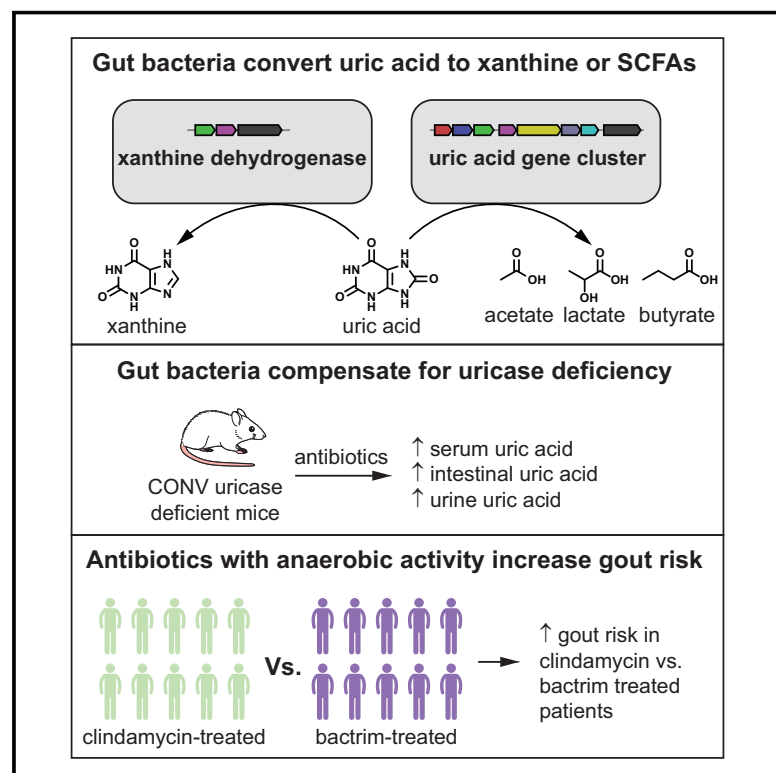
Authors

Yuanyuan Liu, J. Bryce Jarman,
Yen S. Low, ..., Alan C. Pao,
Saurabh Gombar, Dylan Dodd

Correspondence

ddodd2@stanford.edu

In brief

Anaerobic bacteria of the gut microbiome are able to metabolize uric acid, compensating for the uricase deficiency of their host. This conversion of uric acid to xanthine or SCFAs is important for maintaining low levels of uric acid in serum, lowering gout risk.

Highlights

- Anaerobic uric acid metabolism is widespread among the gut microbiota

- Gut bacteria use a conserved gene cluster to convert uric acid to SCFAs

- Microbiota depletion in uricase-deficient mice causes severe hyperuricemia

- Antibiotics with anaerobic coverage increase risk for gout in humans

CellPress

Article

A widely distributed gene cluster compensates for uricase loss in hominids

Yuanyuan Liu,[1] J. Bryce Jarman,[1] Yen S. Low,[2] Hannah E. Augustijn,[3,4] Steven Huang,[5] Haoqing Chen,[1] Mary E. DeFeo,[1,6] Kazuma Sekiba,[1] Bi-Huei Hou,[1] Xiandong Meng,[7] Allison M. Weakley,[7] Ashley V. Cabrera,[7] Zhiwei Zhou,[1] Gilles van Wezel,[4,8] Marnix H. Medema,[3,4] Calyani Ganesan,[9] Alan C. Pao,[9,10,11] Saurabh Gombar,[1,2] and Dylan Dodd[1,6,12,*]

[1]Department of Pathology, Stanford University School of Medicine, Stanford, CA 94305, USA
[2]Atropos Health, Palo Alto, CA, USA
[3]Bioinformatics Group, Wageningen University, Wageningen, the Netherlands
[4]Institute of Biology, Leiden University, Leiden, the Netherlands
[5]Department of Molecular and Cell Biology, University of California, Berkeley, Berkeley, CA 94720, USA
[6]Department of Microbiology and Immunology, Stanford University School of Medicine, Stanford, CA 94305, USA
[7]ChEM-H Institute, Stanford University, Stanford, CA 94305, USA
[8]Netherlands Institute of Ecology, Wageningen, the Netherlands
[9]Division of Nephrology, Department of Medicine, Stanford University School of Medicine, Stanford, CA 94305, USA
[10]Department of Urology, Stanford University School of Medicine, Stanford, CA 94305, USA
[11]Veterans Affairs Palo Alto Health Care System, Palo Alto, CA 94304, USA
[12]Lead contact
*Correspondence: ddodd2@stanford.edu
https://doi.org/10.1016/j.cell.2023.06.010

SUMMARY

Approximately 15% of US adults have circulating levels of uric acid above its solubility limit, which is causally linked to the disease gout. In most mammals, uric acid elimination is facilitated by the enzyme uricase. However, human uricase is a pseudogene, having been inactivated early in hominid evolution. Though it has long been known that uric acid is eliminated in the gut, the role of the gut microbiota in hyperuricemia has not been studied. Here, we identify a widely distributed bacterial gene cluster that encodes a pathway for uric acid degradation. Stable isotope tracing demonstrates that gut bacteria metabolize uric acid to xanthine or short chain fatty acids. Ablation of the microbiota in uricase-deficient mice causes severe hyperuricemia, and anaerobe-targeted antibiotics increase the risk of gout in humans. These data reveal a role for the gut microbiota in uric acid excretion and highlight the potential for microbiome-targeted therapeutics in hyperuricemia.

INTRODUCTION

Uric acid is an intermediate in purine degradation in mammals. In most mammals, uric acid is converted to freely soluble allantoin via urate oxidase (uricase), which is then excreted via the kidney. However, early in hominid evolution, progressive mutations occurred in the uricase gene, decreasing its activity until uricase function was completely lost.[1] Although uricase pseudogenization may have been beneficial for our ancestors,[1–3] in modern times it has become a liability. Approximately 14.6% of the US population has hyperuricemia (defined by plasma levels of uric acid > 6.8 mg/dL [> 0.4 mM]) and 3.9% have clinical features of gout, a painful inflammatory arthritis caused by precipitation of uric acid crystals.[4] Therapies for gout include inhibitors of xanthine oxidase—upstream of uric acid in the purine metabolism pathway—or drugs that block reabsorption of uric acid in the proximal renal tubule. Most of these medications suffer either from poor efficacy, poor compliance, or intolerable side effects, thus new therapies for gout are needed.

Three independent lines of evidence suggest that the gut is an important site for uric acid elimination in humans. First, radioisotope studies in healthy individuals revealed that ∼1/3 of uric acid is disposed from the gut; in patients with kidney disease, this proportion rises to ∼2/3 (Figure 1A).[5] Second, variants in the intestinal/renal transporter ABCG2 diminish intestinal uric acid elimination,[6] and *ABCG2* mutations are risk factors for hyperuricemia and gout.[7,8] Third, extensive literature exists for a parallel process involving the excretion of oxalate via bacterial metabolism in the gut.[9] Certain strains of bacteria, such as *Oxalobacter formigenes*, consume oxalate in the gut and limit kidney stone formation.[10] Although it is presumed that bacteria in the gut break down uric acid to products that are absorbed and excreted by the host,[5] uric acid metabolism by commensal gut bacteria has not been studied.

Here, we report that a large number of gut bacteria consume uric acid anaerobically, converting it to either xanthine or lactate and the short chain fatty acids (SCFAs), acetate and butyrate. Transcriptional profiling and genetics reveal a gene cluster that
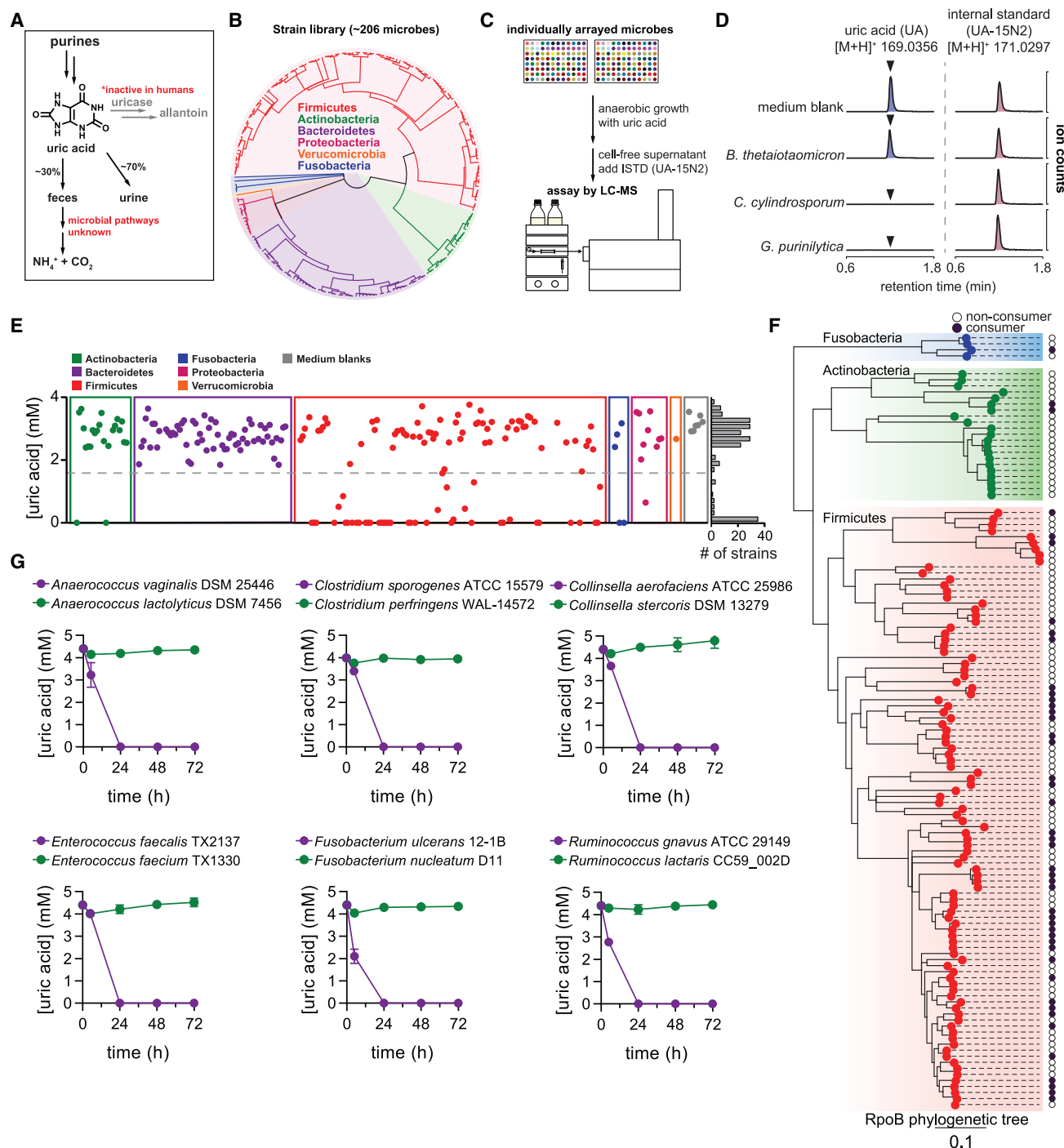
Figure 1. Anaerobic uric acid metabolism is widespread among human gut bacteria

(A) Overview of purine metabolism in humans.

(B) Phylogenetic distribution of human gut bacteria in the strain library used for this study.

(C) Overview of experimental approach to screen for uric acid metabolism.

(D) Extracted ion chromatograms for uric acid and the uric acid internal standard (ISTD; [15N2]-uric acid) in medium blank and after incubation with a non-consumer (*B. thetaiotaomicron*) and two known purine-consuming bacteria (*C. cylindrosporum* and *G. purinilytica*).

(E) Results from uric acid screen in rich medium, grouped by phylum. Each dot represents a single bacterial strain. The frequency of strains is shown on the right of the plot.

(legend continued on next page)

is required for conversion of uric acid to SCFAs and is widely distributed across phylogenetically distant bacterial taxa. We find that human gut bacteria compensate for the loss of uricase in genetic and chemically induced mouse models and that antibiotics targeting anaerobic bacteria, which would ablate gut bacteria, increase the risk for developing gout in humans. Together, our findings uncover a previously unknown mechanism by which gut bacteria contribute to uric acid homeostasis in the host.

RESULTS

Anaerobic uric acid metabolism is widespread among gut bacteria

Although uric acid metabolism is well known to occur among aerobic bacteria, anaerobic uric acid metabolism has been described in only a few purine-degrading bacteria isolated from soil. Early biochemical studies with *Clostridium cylindrosporum* established the enzymatic activities involved in anaerobic purine metabolism[11–15]; however, the identity of genes supporting this purinolytic pathway is not known.[16–18] Thus, no marker genes are available to query gut bacterial genomes for uric acid metabolism.

To identify uric-acid-consuming gut bacteria, we cultured our phylogenetically diverse human gut bacterial strain library (Figure 1B) with uric acid and quantified remaining uric acid by isotope dilution using liquid chromatography-mass spectrometry (LC-MS) (Figure 1C). We first validated the assay, showing that known purine-degrading bacteria (*C. cylindrosporum* and *Gottschalkia purinilytica*)[19] consume uric acid, whereas *Bacteroides thetaiotaomicron* does not (Figure 1D). Next, we found that uric acid consumption was remarkably widespread among gut bacteria, with over 1/5 (46/206) of strains in our library consuming >50% of uric acid after 48 h of anaerobic growth (Figure 1E). Uric acid consumption was distributed across 4 phyla (Actinobacteria, Firmicutes, Fusobacteria, and Proteobacteria), but notably absent in the Bacteroidetes. We repeated this screen with an expanded library of strains under carbohydrate-limiting conditions (Figure S1A). Results from the second screen: (1) confirmed findings for most of the organisms in the first screen; (2) identified additional uric-acid-consuming strains, bringing the total to 59/240 strains tested; and (3) revealed that some strains consume more uric acid in the absence of carbohydrates (Figure S1B).

By combining results from the two screens, we found that uric acid consumption varies widely, even among closely related bacteria (Figure 1F). We cultured a subset of related species with uric acid and confirmed that uric acid metabolism is not strictly conserved, even within closely related bacterial lineages (Figure 1G). Although we cannot rule out that laboratory adaptation may have selected for loss of uric acid metabolism, we note that several type strains—more likely to be highly passaged—

retain uric acid metabolism activity. These findings suggest that the capacity to consume uric acid may have been gained or lost multiple times during bacterial evolution.

Gut bacteria convert uric acid into xanthine and short chain fatty acids

Having identified numerous uric-acid-consuming gut bacteria, we next asked what is the metabolic fate of uric acid in these bacteria? We found that some strains accumulated xanthine in supernatants when consuming uric acid (Figure S1C). However, these xanthine-producing strains represented just a subset of uric acid consumers, indicating that many bacteria produce other yet unidentified metabolites.

Next, we performed stable isotope tracing in xanthine-producing and non-producing strains using uniformly labeled [$^{13}C_5$]-uric acid (Figure 2A). Over time, the xanthine-producing strain *Blautia sp.* KLE 1732 consumed [$^{13}C_5$]-uric acid and the M + 5 isotopolog of xanthine accumulated in culture supernatants (Figure 2B). In contrast, while the xanthine non-producing strain, *C. sporogenes* ATCC 15579, consumed [$^{13}C_5$]-uric acid, M + 5 xanthine did not accumulate (Figure 2C). Rather, we detected an increase in the M + 2 isotopologs of acetate and butyrate, suggesting that *C. sporogenes* converts uric acid to SCFAs (Figure 2C). M + 2 acetate also appeared in the *Blautia sp.* KLE 1732 cultures, but the levels were equivalent in both unlabeled and labeled uric-acid-supplemented cultures (Figure 2B), thus reflecting natural isotope abundances within acetate produced during growth (Figure S2A). Therefore, for all strains tested, we subtracted isotopologs during growth with unlabeled uric acid from isotopologs during growth with labeled uric acid. Our results identify two routes for uric acid metabolism among gut bacteria, (1) conversion of uric acid to xanthine and (2) more complete breakdown of uric acid where carbons are diverted to lactate and the SCFAs, acetate and butyrate (Figures 2D and 2E). By comparing uric acid metabolism in rich and more limited media, we found that nutrient availability influences uric acid consumption to different extents among phylogenetically diverse bacteria (Figure S2B).

Identification of a uric-acid-inducible gene cluster required for anaerobic uric acid metabolism

To identify genes involved in uric acid conversion to SCFAs, we cultured three phylogenetically distinct organisms (*C. sporogenes*, *L. saccharolytica*, and *C. aerofaciens*) in rich medium, with or without uric acid, and performed RNA sequencing (RNA-seq) analysis (Figure 3A). We found five uric-acid-inducible genes (*ygeX*, *ygeY*, *ygeW*, *ygfK*, and *ssnA*) shared across the three bacteria (Figure 3B) that were among the most highly induced genes (Figure 3C; Table S1) and mapped to discrete gene clusters shared across the three bacteria (Figure 3D). Notably, annotations for these genes derive from *Escherichia coli*, where they code for enzymes

---

(F) Phylogenetic distribution of uric-acid-consuming bacteria within the Actinobacteria, Fusobacteria, and Firmicutes phyla. Dark purple dots represent strains that consume >50% of the uric acid. Only those strains for which assembled genomes are available were included.

(G) Uric acid consumption in closely related bacteria during growth in rich media. For (D) and (E), data represent the results from a single experiment. For (G), data represent the mean ± SDs of n = 3 biological replicates.

See also Figure S1.
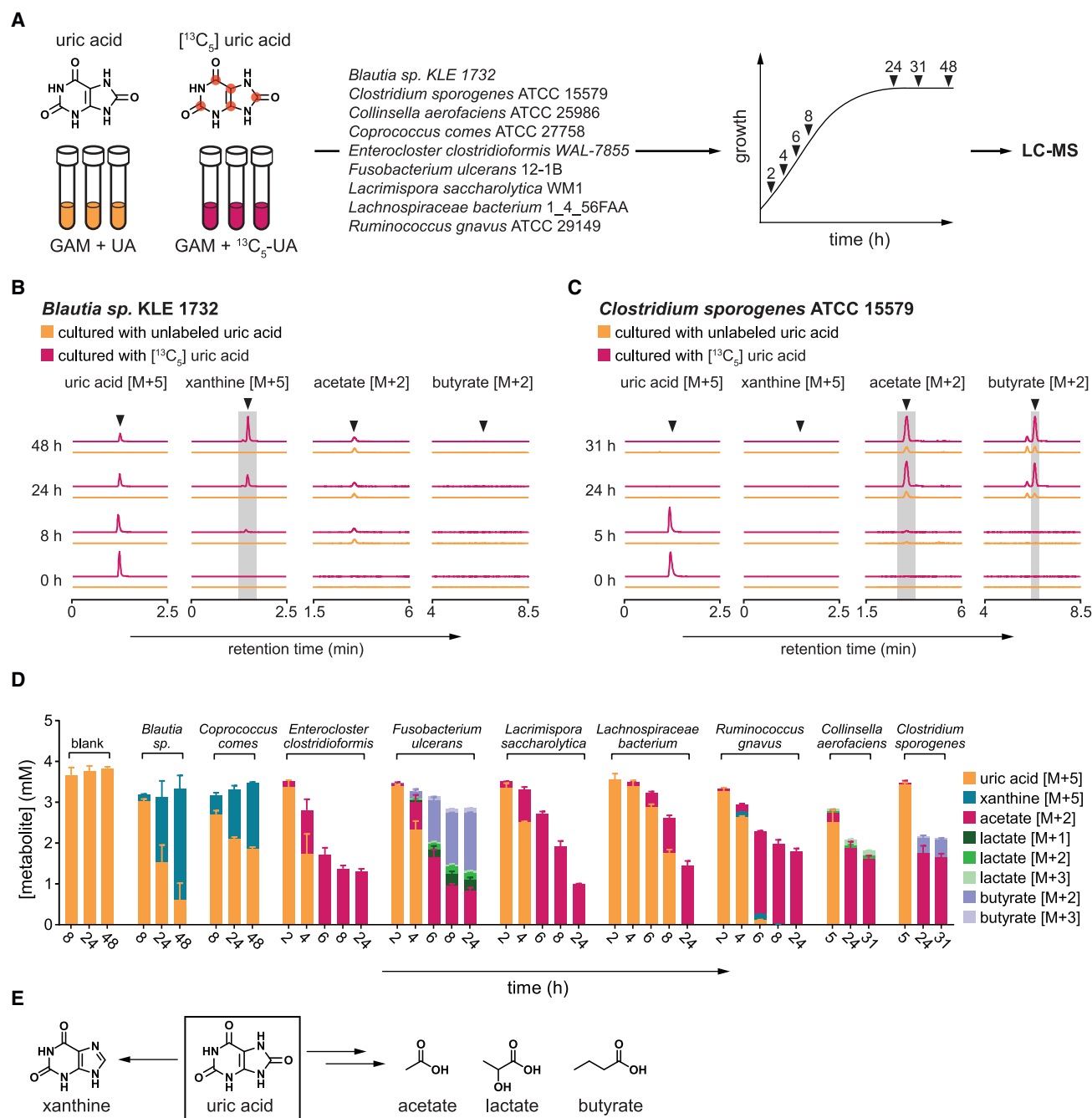
Figure 2. Gut bacteria convert uric acid into xanthine or lactate and short chain fatty acids

(A) Overview of stable isotope tracing. Bacteria were cultured in rich media containing either unlabeled or uniformly labeled [$^{13}C_5$] uric acid and metabolites were quantified at indicated times by LC-MS.

(B and C) Extracted ion chromatograms for labeled substrates or products when (B) *Blautia sp.* KLE 1732 or (C) *Clostridium sporogenes* ATCC 15579 was cultured with labeled or unlabeled uric acid.

(D) Labeled substrates and products detected in cell-free culture supernatants of all nine bacteria studied.

(E) Uric acid is converted either to xanthine or lactate and the SCFAs acetate and butyrate. For (B) and (C), arrows indicate expected retention times for indicated compounds. For (C), the peak eluting 0.3 min before butyrate [M + 2] was identified as isobutyrate [M + 2]. For (B) and (C), experiments were performed in triplicate and representative data are shown. For (D), data represent the mean ± SDs of n = 3 biological replicates. Strains include: *Blautia sp.* KLE 1732, *Coprococcus comes* ATCC 27758, *Enterocloster clostridioformis* WAL-7855, *Fusobacterium ulcerans* 12-1B, *Lacrimispora saccharolytica* WM1, Lachnospiraceae bacterium 1_4_56FAA, *Ruminococcus gnavus* ATCC 29149, *Collinsella aerofaciens* ATCC 25986, and *Clostridium sporogenes* ATCC 15579. GAM, Gifu anaerobic medium. See also Figure S2.
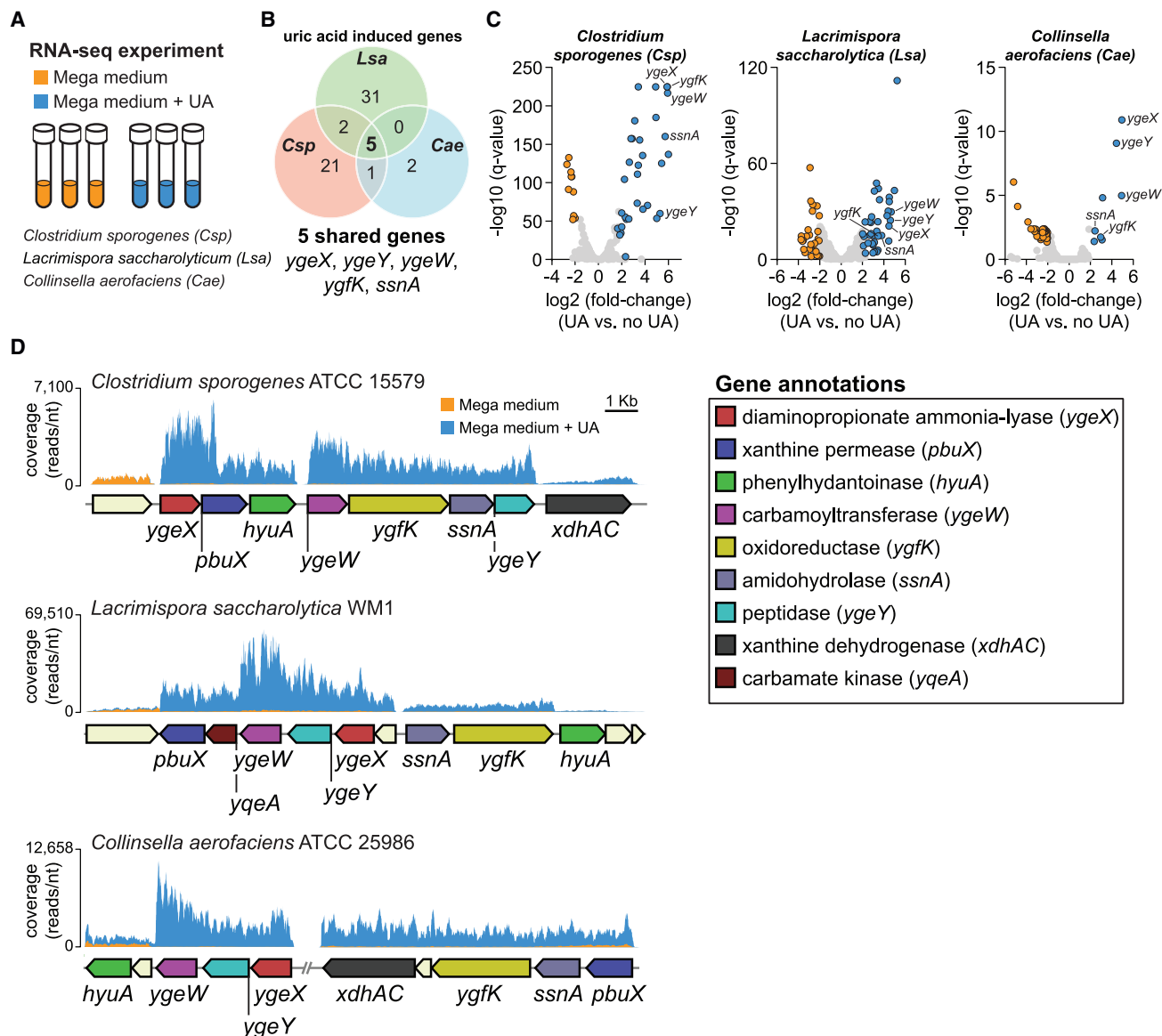
Figure 3. RNA-seq reveals a uric-acid-inducible gene cluster in gut bacteria

(A) Overview of experimental design. Three organisms (*C. sporogenes*, *L. saccharolytica*, and *C. aerofaciens*) were cultured in rich medium, with and without supplemental uric acid, and transcriptomes were analyzed by RNA-seq.

(B) Venn diagram showing significantly induced genes for all three organisms (false discovery rate [FDR]-corrected p value [q value] < 0.05, fold-change > 4).

(C) Volcano plots showing differentially regulated genes in the three organisms. Cutoffs include FDR corrected p value (q value) < 0.05 and |fold-change| > 4. Each dot represents a single gene. Blue dots represent genes that are induced, and orange dots represent genes that are repressed when uric acid is present.

(D) Genomic context and RNA-seq coverage for conserved uric-acid-inducible genes. For RNA-seq experiments, three biological replicates were performed for each condition. For (D), representative data are shown.

whose activities are predicted at the family level, but for which substrate specificities and cellular roles are unknown. Putative annotations for these gene products include ammonia lyase (YgeX), peptidase (YgeY), carbamoyl transferase (YgeW), oxidoreductase (YgfK), and amidohydrolase (SsnA), which are enzymes that may reduce and cleave bonds present in uric acid. These findings reveal a conserved set of uric-acid-inducible genes that are shared across diverse gut bacterial taxa.

Genetics and stable isotope tracing in *C. sporogenes* revealed that mutations either partially (*ygeX*, *pbuX*, *hyuA*, *ygeW*, *ygfK*, *ssnA*, *ygeY*) or completely (*xdhAC*) blocked uric acid metabolism (Figures 4A and 4B). Neither labeled acetate nor labeled butyrate were detected in culture supernatants of any of the mutant strains (Figure 4B). These findings provide evidence that the uric-acid-inducible genes in *C. sporogenes* are required for conversion of uric acid to SCFAs, including acetate and butyrate.

Figure 4. Uric-acid-inducible genes are required for conversion of uric acid to short chain fatty acids

(A) Individual mutants (indicated by red triangles) were generated in *C. sporogenes* using the ClosTron system.

(B) Stable isotope tracing in wild-type and mutant *C. sporogenes* strains. For (B), data represent the mean ± SDs of n = 3 biological replicates.
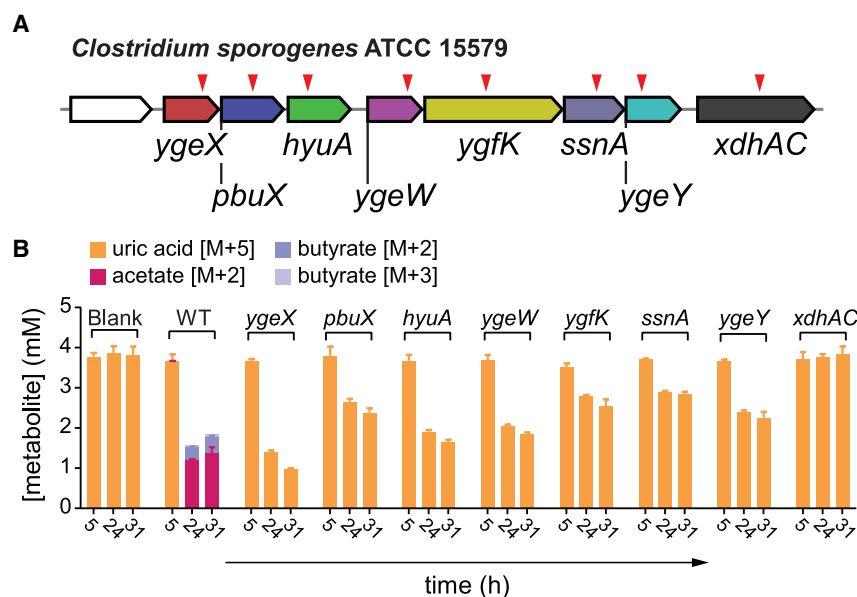
Uric-acid-inducible genes are widely distributed across human gut bacteria

Phylogenetic analyses revealed that the uric acid metabolic genes are broadly distributed across gut bacteria, occurring within 4 phyla, 19 families, and 21 genera (Figure 5A; Table S2). The presence of uric acid metabolic genes showed strong concordance with the capacity for uric acid metabolism and explained differences in uric acid consumption between phylogenetically related bacteria in Figure 1G (Table S2). We also found that these uric acid metabolic genes mapped to conserved gene clusters across broad taxonomic lineages (Figure 5B). Those bacteria that did not carry the genes, but consumed uric acid, included (1) previously studied purine-degrading bacteria (*Clostridium cylindrosporum* and *Gottschalkia purinilytica*) known to convert uric acid to acetate, but likely involving a different set of genes, and (2) bacteria that we found convert uric acid to xanthine (Figure S3A). These xanthine-producing bacteria harbor putative xanthine dehydrogenase genes (Figure S3B), and we conclude that these strains likely convert uric acid to xanthine in a single step involving xanthine dehydrogenase.

Escherichia coli converts uric acid to acetate anaerobically

The *E. coli* genome harbors a gene cluster containing most of the uric-acid-inducible genes identified in our study. *E. coli* has previously been demonstrated to consume uric acid under anaerobic conditions in a mechanism requiring formate and involving several genes, including *aegA*, *ygfT*, and *ygeV*.[20] Of note, the *ygfT* and *ygeV* genes map to the same gene locus as the *ygeW*, *ygeX*, *ygeY*, *hyuA*, *ygfK*, and *ssnA* genes identified in our study (Figure 6A). However, the role of these latter genes in uric acid metabolism by *E. coli* has not been studied.

Despite containing the genes for uric acid metabolism, under the conditions of our initial screen, *E. coli* was not identified as a uric-acid-consuming bacterium (Figure 6B). To test whether

E. coli consumes uric acid under anaerobic conditions, we cultured the MG1655 strain in 11 different anaerobic media supplemented with uric acid and monitored uric acid over time by LC-MS. Consistent with results from our initial screen, uric acid was not substantially consumed in mega media (Figure 6C). However, we identified four different media which supported complete consumption of uric acid (Figure 6C). Our findings suggest that *E. coli* consumes uric acid and that nutrient availability dramatically influences this phenotype.

Next, we created markerless deletion mutants in *E. coli* MG1655 and used stable isotope tracing to quantify uric acid metabolism during growth in modified Gifu anaerobic medium (GAM.M). Under these conditions, the wild-type *E. coli* strain consumed all the uric acid within 48 h, and culture supernatants accumulated M + 2 acetate (Figure 6D). By comparison, the mutant strains were partially blocked in uric acid metabolism and none of the cultures accumulated M + 2 acetate (Figure 6D). These findings provide evidence that under certain nutrient conditions, *E. coli* degrades uric acid to acetate in a pathway that involves *ygeW*, *ygeX*, *ygeY*, *hyuA*, *ygfK*, and *ssnA*.

A previous study identified *aegA* and *ygfT* as genes involved in formate-dependent uric acid metabolism in *E. coli*.[20] These two genes encode putative oxidoreductases that harbor iron sulfur cluster binding domains and a pyridine-dependent oxidoreductase domain (Figure 6E). AegA and YgfT have been proposed to accept electrons from formate dehydrogenase and transfer them to NADP$^+$ or directly to uric acid.[20] We found that YgfK also shares two of the three domains present in AegA and YgfT (Fer4_20 and Pyr_redox_2), suggesting that these three enzymes might perform analogous reactions under different nutrient conditions. We found that during growth in GAM.M, uric acid highly induced the expression of *ygfK* and *ygfT* but had only a modest influence on *aegA* expression (Figure 6F). These results suggest that both *ygfT* and *ygfK* are likely involved in uric acid metabolism under these conditions, whereas *aegA* is not.

Comparison of two facultative anaerobes (*E. coli* and *Enterococcus faecalis*) showed that uric acid was consumed only under anaerobic conditions (Figure S4). These findings, coupled with the observation that most of the strains harboring uric acid genes are facultative or obligate anaerobes, lead us to reason that the genes identified in our study are likely to be specific to anaerobic uric acid metabolism.
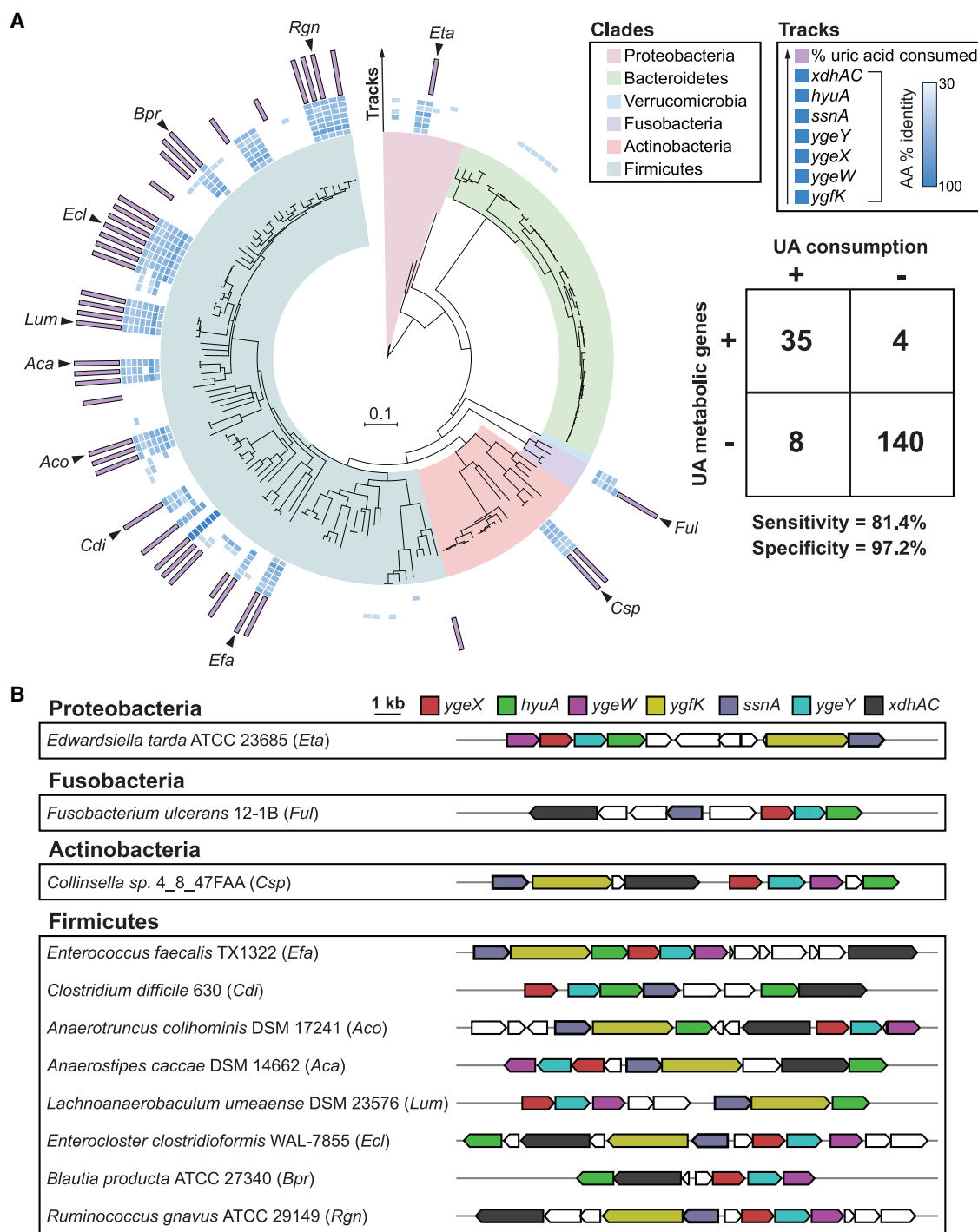
Figure 5. Uric acid gene cluster is conserved across uric-acid-consuming gut bacteria

(A) RpoB phylogenetic tree for strains screened for uric acid metabolism in this study. Only those strains with assembled genomes are included (n = 187). Clades are colored by phylum. Inner blue shaded tracks represent the % amino acid identity of protein homologs identified from BLASTp searches using *C. sporogenes* proteins as queries. The outer-most track represents the % uric acid consumed by each strain. Uric acid consumption values are only shown for strains with ≥50% uric acid consumption. Table shows the number of bacteria positive or negative for genes (cutoff ≥ 5 of 7 genes) vs. positive or negative for uric acid consumption (cutoff ≥ 50% uric acid consumption). The cutoff of ≥ 5 of 7 genes was determined by analyzing sensitivity and specificity at different gene cutoff values (Table S2).

(B) Genomic context of uric acid metabolic genes from representative uric-acid-consuming strains corresponding to black arrows in (A).

See also Figure S3.
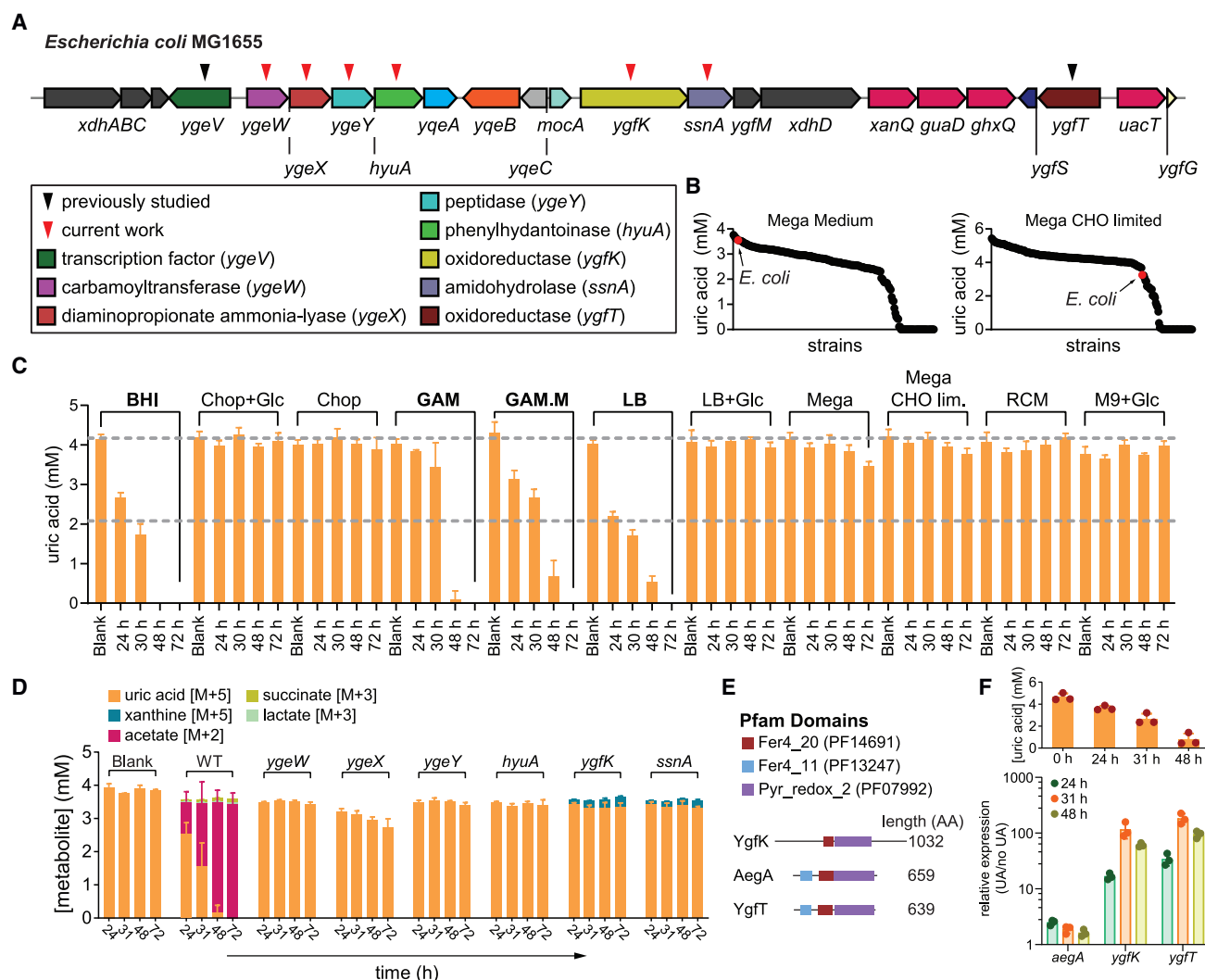
Figure 6. Nutrient dependence of *E. coli* uric acid metabolism and role of genes in conversion of uric acid to acetate

(A) Genomic context for uric acid metabolic genes in *E. coli*. Black triangles indicate previously studied genes, and red triangles indicate genes targeted in this study.

(B) Results from uric acid metabolism screens under carbohydrate (CHO) replete (left) or CHO limited (right) conditions. Strains are ordered by amount of uric acid remaining and *E. coli* is indicated by a red dot.

(C) Uric acid metabolism by *E. coli* under different nutrient conditions.

(D) Stable isotope tracing in wild-type and mutant *E. coli* strains. Strains were cultured in modified Gifu anaerobic medium containing either labeled or unlabeled uric acid. Labeled substrates and products were quantified by LC-MS.

(E) Pfam domains for YgfK and two gene products (AegA and YgfT) previously shown to be involved in uric acid metabolism by *E. coli*.

(F) Relative expression of *ygfK*, *aegA*, and *ygfT* in uric-acid-supplemented vs. non-supplemented conditions. Uric acid remaining in the medium is shown in the upper panel. For (B), data in the two panels represent the results from a single experiment per condition. For (C), (D), and (F), data represent the mean ± SDs of n = 3 biological replicates.

See also Figure S4.

Gut bacteria compensate for uricase deficiency in mice

Unlike humans, mice have a functional uricase enzyme (also known as urate oxidase [*Uox*]), and wild-type mice have lower levels of plasma uric acid compared with humans.[21] To investigate the role of the microbiome in hyperuricemia, we used two mouse models: (1) mice carrying a targeted mutation in the *Uox* gene[22] and (2) chemical inhibition of uricase with oxonic acid (Figure 7A). *Uox* knockout (*Uox*^{−/−}) mice are hyperuricemic,

accumulate uric acid crystals in the kidney, and suffer from early lethality.[22] To overcome perinatal lethality, we provided allopurinol (a xanthine oxidase inhibitor) in the drinking water during breeding and after weaning (Figure 7A).[22] We also confirmed results from prior studies,[23] showing that addition of the xanthine oxidase inhibitor (allopurinol) in the blood collection tube limits false *in vitro* elevation of uric acid (Figure S5A). Thus, we used this sampling method in all our mouse experiments.
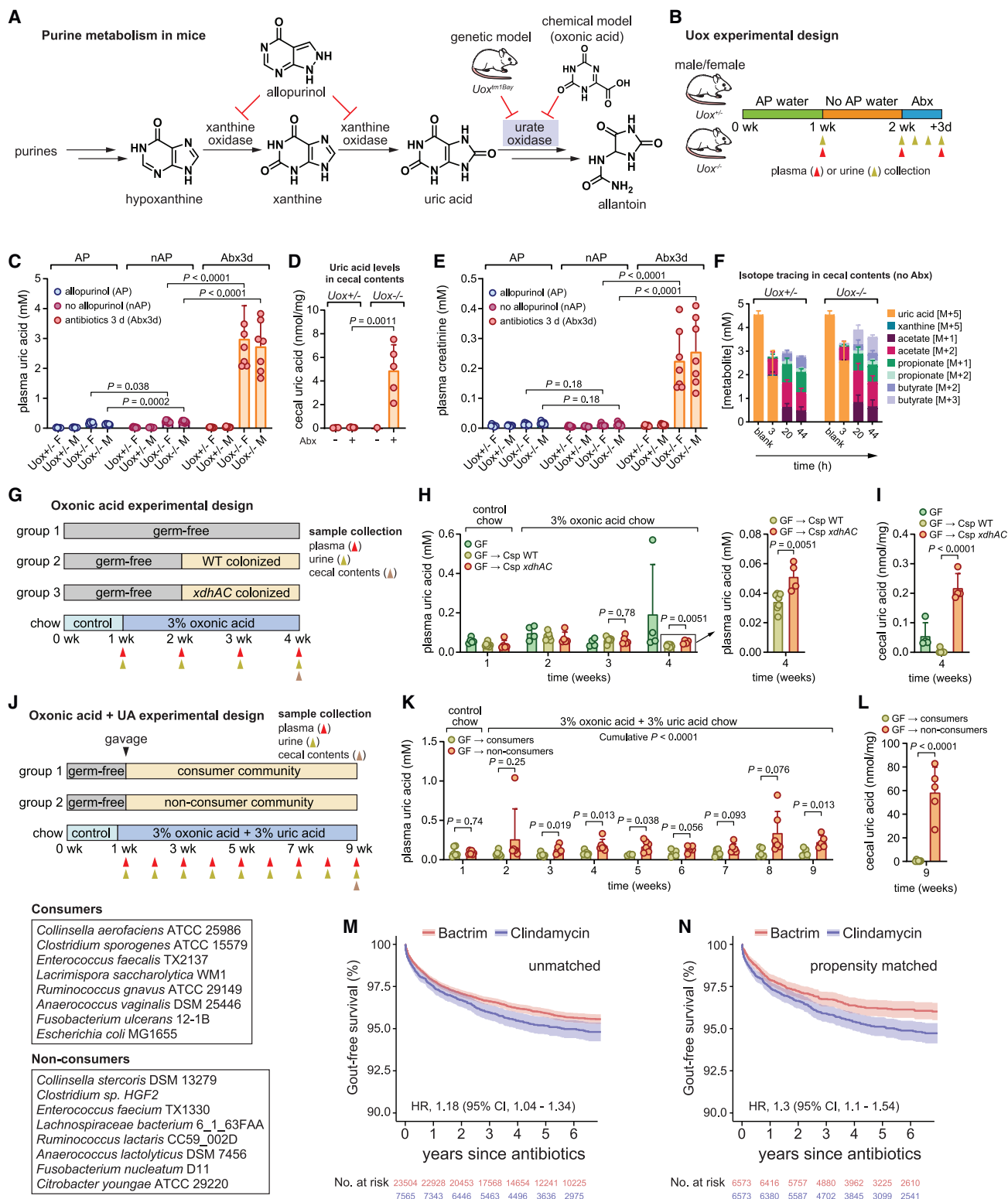
Figure 7. Gut bacteria compensate for loss of uricase

(A) Overview of purine metabolism in mice.

(B) Overview of *Uox* mouse experimental design.

(C) Plasma uric acid levels in male and female *Uox*^+/− or *Uox*^−/− mice.

To test whether the gut microbiota can compensate for uricase deficiency, we treated male and female $Uox^{-/-}$ mice and their heterozygous ($Uox^{+/-}$) littermate controls with an antibiotic cocktail and measured serum and urine uric acid concentrations (Figure 7B). Allopurinol treatment had a modest influence on serum and urine uric acid in $Uox^{-/-}$ mice (Figures 7C and S5B); however, antibiotic- treated $Uox^{-/-}$ mice became ill and developed severe hyperuricemia (Figure 7C). Intestinal levels of uric acid in the cecal contents were increased in antibiotic-treated $Uox^{-/-}$ mice, indicating that bacterial depletion diminished intestinal uric acid metabolism (Figure 7D). In the 3 days after antibiotic administration, urine uric acid excretion progressively decreased, suggesting that kidney function was impaired (Figure S5B). Indeed, antibiotic-treated $Uox^{-/-}$ mice showed evidence of acute kidney injury with markedly elevated concentrations of plasma creatinine (Figure 7E) and urea (Figure S5C). This rise in plasma creatinine and urea reflects acute kidney injury, and the combination of acute kidney injury with acute hyperuricemia is reminiscent of acute uric acid nephropathy seen in tumor lysis syndrome in humans.[22]

Cecal contents from both $Uox^{+/-}$ and $Uox^{-/-}$ mice consumed uric acid in vitro, converting it to a mixture of SCFAs (Figure 7F). These findings show that the microbiota of these mice have the capacity to consume uric acid and convert it to SCFAs similar to those we detected for bacteria grown in vitro (Figure 2D). Assembly of shotgun metagenomics reads from cecal contents of $Uox^{+/-}$ and $Uox^{-/-}$ mice identified eight contigs belonging to three separate bacterial families, each containing the uric acid gene cluster (Figures S5D and S5E). This indicates that bacteria harboring the uric acid gene cluster are present within the microbiota of these mice. However, gene cluster abundances or expression was not significantly different between $Uox^{-/-}$ and $Uox^{+/-}$ mice (Figures S5F and S5G). Thus, our metagenomics analysis establishes that bacteria encoding the uric acid genes are present in microbiota colonizing the cecum of Uox mice, although the gene abundance and expression do not differ between $Uox^{+/-}$ and $Uox^{-/-}$ mice.

Next, we adopted a widely used model for chemically induced hyperuricemia[25] to more concretely connect bacterial uric acid metabolism to uric acid levels in the host. In germ-free mice, oxonic acid chow induced modest elevations in plasma and urine uric acid and plasma creatinine (Figures S6A and S6B). By contrast, the oxonic acid and uric acid chow induced severe hyperuricemia, hyperuricosuria, and elevated plasma creatinine (Figures S6C and S6D). This latter model phenocopies microbiota depletion in uricase-deficient mice.

We then compared germ-free mice and mice mono-colonized with either wild-type *C. sporogenes* or its xanthine dehydrogenase (*xdhAC*) mutant, which does not consume uric acid in vitro (Figure 4B). Mice were fed a control diet for 1 week, then switched to oxonic acid chow for 1 week prior to colonization (Figure 7G). Despite the mild hyperuricemia induced by this diet, we detected a significant decrease in uric acid levels in both the plasma and in the cecal contents for wild-type compared with *xdhAC*-colonized mice after 2 weeks (Figures 7H and 7I). Urine uric acid levels were not significantly different between groups of mice (Figure S6E). Next, we compared gnotobiotic mice colonized with bacterial communities consisting of uric-acid-consuming bacteria or phylogenetically matched non-uric-acid-consuming bacteria (Figure 7J). These mice were fed a control diet for 6 days and then switched to a diet containing both oxonic acid and uric acid. Mice colonized with a consumer community had lower uric acid levels in the plasma and cecal contents (Figures 7K and 7L) and in the urine (Figure S6F) compared with non-consumer-colonized mice. Together, these experiments establish that bacterial uric acid metabolism in the gut reduces uric acid levels in the host.

Antibiotics targeting anaerobic gut microbes increase risk for gout in humans

Given our findings that antibiotic treatment induced severe hyperuricemia in $Uox^{-/-}$ mice, we next asked whether antibiotic treatment might be a risk factor for gout in humans. To address this, we compared two commonly prescribed oral antibiotics: (1) clindamycin, which is known to target both aerobic and anaerobic microbes, and (2) trimethorprim/sulfamethoxazole (Bactrim), which targets aerobic microbes. We hypothesized that clindamycin might uniquely disrupt uric-acid-degrading gut bacteria because they are anaerobic microbes. We conducted a retrospective cohort study using electronic health records collected from the Stanford Health Care system between 2015 and 2019. We examined all adult patients (regardless of gout

(D) Cecal uric acid levels in $Uox^{+/-}$ or $Uox^{-/-}$ mice, with or without antibiotic treatment.

(E) Plasma creatinine levels in male and female $Uox^{+/-}$ or $Uox^{-/-}$ mice.

(F) Isotope tracing in cecal contents of non-antibiotic-treated $Uox^{+/-}$ or $Uox^{-/-}$ mice.

(G) Overview of oxonic-acid-only experiment with gnotobiotic C57Bl/6 mice. WT, wild type *C. sporogenes*; *xdhAC*, xanthine dehydrogenase mutant *C. sporogenes*.

(H) Plasma uric acid levels in GF, WT, or *xdhAC*-colonized mice. Panel at right represents a zoomed-in view of the final time point.

(I) Cecal uric acid levels in GF, WT, or *xdhAC*-colonized mice.

(J) Overview of oxonic acid + uric acid experiment with gnotobiotic C57Bl/6 mice. Community members are indicated in the boxes.

(K) Plasma uric acid levels in non-consumer or consumer-colonized mice.

(L) Cecal uric acid levels in non-consumer or consumer-colonized mice.

(M) Kaplan-Meier survival curves for unmatched patients treated with oral Bactrim or clindamycin ($\geq$ 5-day course) with a diagnosis of gout as the end point.

(N) Kaplan-Meier survival curves for propensity score matched patients treated with Bactrim or clindamycin ($\geq$ 5-day course) with a diagnosis of gout as the end point.

For (B), (G), and (J), timing of sample collection is indicated with gold (urine), red (plasma), or brown (cecal contents) arrows. For (C) and (E), data represent mean ± SDs from n = 7–8 mice per group. For (D), data represent mean ± SDs from n = 5 mice (antibiotic-treated $Uox^{+/-}$ or $Uox^{-/-}$ mice) or pools for non-antibiotic-treated mice (6 mice into 3 pools for $Uox^{+/-}$ and 3 mice into 1 pool for $Uox^{-/-}$). For (F), data represent mean ± SDs from n = 4 mice ($Uox^{+/-}$) or n = 8 mice ($Uox^{-/-}$). For (H) and (I), data represent mean ± SDs from n = 5–7 mice per group. For (K) and (L), data represent mean ± SDs from n = 6 mice per group. p values are from two-tailed unpaired Student's t tests. AP, allopurinol; nAP, no allopurinol; Abx, antibiotics. The mouse schematic in (A) and (B) was adapted from Dodd et al.[24]

See also Figures S5, S6, and S7.

history) and compared rates of incident gout diagnosis in the years following treatment with ≥5 days of oral clindamycin (N = 7,565) vs. ≥5 days of oral Bactrim (N = 23,504). The two groups were similar in age (53.1 vs. 53.4 years), sex distribution (59.6% vs. 59.1% female), and co-morbid illness (average comorbidity score 3.2 vs. 3.5) (Table S3). In the unmatched cohort, patients treated with clindamycin had a higher risk for developing a diagnosis of gout compared with patients treated with Bactrim (hazard ratio, 1.18, 95% confidence interval [CI], 1.04–1.34, p = 0.0091) (Figure 7M). After propensity score matching (N = 6,573 for clindamycin or Bactrim), the risk for a gout diagnosis increased for patients treated with clindamycin compared with those treated with Bactrim (hazard ratio, 1.3, 95% CI, 1.1–1.54, p = 0.0026) (Figure 7N). These findings suggest that disruption of the anaerobic gut microbiota by broad-spectrum antibiotics with anaerobic activity increases the risk of developing gout in humans.

To address whether microbiota depletion influences fecal uric acid levels, we re-analyzed metabolomics data from the Food and Resulting Microbial Metabolites (FARMM) study exploring the role of diet in microbiome metabolite recovery after disruption with antibiotics and polyethylene glycol.[26] We found that microbiota depletion resulted in dramatically elevated fecal levels of uric acid (Figure S7A). Fecal uric acid levels rapidly returned to baseline in subjects fed a vegan or omnivore diet, but those fed a fiber-free synthetic diet (exclusive enteral nutrition; EEN) showed a protracted recovery, with persistent elevations of fecal uric acid throughout the recovery phase (Figure S7A). To explore whether the uric acid gene cluster varied in abundance across FARMM study subjects, we used gutSMASH[27,28] to identify 782 gene clusters from human gut bacterial reference genomes and mapped metagenomic reads from study subjects to 107 representative gene clusters using BiG-MAP.[29] The abundance of uric acid genes was significantly reduced post antibiotic treatment in study subjects fed an EEN diet compared with study subjects fed an omnivore or a vegan diet (Figure S7B). The authors of the FARMM study found that bacteria from the Firmicutes phylum showed delayed recovery in the EEN group. Our findings are consistent with this observation, showing that differences in uric acid gene cluster abundance between EEN and omnivore/vegan groups are largely driven by members of the Firmicutes phylum, notably the Oscillospiraceae, Lachnospiraceae, Peptostreptococcaceae, and Clostridiaceae families (Figure S7C, yellow boxes). These results suggest that a lack of dietary fiber following microbiome perturbation imparts a sustained dysregulation of uric acid metabolism in the gut.

DISCUSSION

Uric acid is one of the most abundant nitrogenous compounds on the planet, being a key intermediate in purine metabolism.[30] Although evidence of aerobic uric acid metabolism can be found across all domains of life, anaerobic uric acid metabolism has been studied in only a handful of bacteria isolated from soil or marine sediments.[31] Here, we find that anaerobic uric acid metabolism is widespread among members of the human gut microbiome, occurring in ~1/5 of bacteria from 4 of 6 major phyla. In contrast to aerobic pathways that rely on oxygen-dependent uri-

case to initiate uric acid metabolism, we find that anaerobic pathways break down uric acid through action of uncharacterized ammonia lyase, peptidase, carbamoyl transferase, and oxidoreductase enzymes. The genes encoding these enzymatic functions map to a conserved gene cluster that is broadly distributed across distantly related bacterial taxa and are required for anaerobic uric acid metabolism to lactate and SCFAs. Intriguingly, previously characterized purine-degrading Clostridia (e.g., *G. purinilytica*, *G. acidiurici*, and *C. cylindrosporum*) do not encode these genes,[16–18] suggesting that distinct pathways for anaerobic uric acid metabolism evolved independently among bacteria. However, the uric acid genes identified in our study are highly predictive of uric acid metabolism activity in gut bacteria, indicating that this gene cluster encodes a predominant pathway for anaerobic uric acid metabolism in the gut. A recent study also identified uric-acid-degrading gut bacteria, the same set of genes, and demonstrated that gut bacteria influence uric acid levels in the host, thus reinforcing our conclusions.[32]

In most mammals, purines are degraded via uricase to freely soluble allantoin, which is excreted in the urine, however uricase was inactivated early in hominid evolution. One prominent hypothesis for why uricase was inactivated suggests uricase may be a thrifty (pseudo)gene. Uricase inactivation occurred gradually over nearly 50 million years, with full inactivation occurring in the early Miocene.[1] Notably, this coincided with global climatic cooling, with rainforests receding toward the equator. Consequently, frugivorous apes underwent periods of starvation, especially during cooler winter months. Studies in mice and rats have shown that loss or inhibition of uricase (1) increases fat storage from fructose, (2) limits beta-oxidation of fats, (3) stimulates gluconeogenesis, and (4) increases blood pressure. These studies provide evidence of uricase as a "thrifty gene," the inactivation of which promoted survival of our ancestors during times of starvation.[33] Our results suggest that the gut microbiota play a compensatory role for uricase loss, enabling homeostatic control over uric acid levels. The implications of this are that loss of uric-acid-consuming bacteria may explain the high prevalence of hyperuricemia and gout in industrialized nations.

Our study provides insights into the role of the gut microbiota in hyperuricemia and gout, two common disorders affecting the US population. There are two important implications of these results. First, antibiotic therapies that might disrupt the gut microbiota should be carefully considered in patients predisposed to gout. If antibiotics are administered to these patients, a low fiber diet may cause a protracted return to normal uric acid metabolism in the gut. Second, approaches to promote uric acid metabolism in the gut represent potentially important therapies for treating patients with hyperuricemia. Along these lines, recent studies have shown that oral (non-absorbable) enzyme therapy with recombinant uricase reduces plasma uric acid concentration in uricase-deficient mice[34] and decreases plasma concentration in healthy volunteers.[35] The uric acid pool is distributed across different body compartments, which include the plasma, joints, kidney, and intestines, the latter two being primary excretion routes mediated by bi-directional transporters.[36] It is thought that enzymatic degradation of intestinal uric acid affects equilibrium of the uric acid pool, diminishing overall

hyperuricemia.[34] We envision that live biotherapeutic products consisting of uric-acid-consuming bacteria could also be an important therapeutic modality to treat hyperuricemia and gout.

Limitations of the study

Uricase-deficient mice develop severe hyperuricemia, akin to tumor lysis syndrome in humans. Given the gradual loss of uricase during hominid evolution, it is likely that adaptive mechanisms appeared to regulate uric acid levels. Selection for uric-acid-consuming gut bacteria may have been one such adaptive mechanism; however, further studies are needed to test whether uric-acid-consuming bacteria are enriched in uricase-deficient mammals and how microbial dysbiosis may contribute to hyperuricemia and gout. Our finding that patients given antibiotics with anaerobic activity have an increase in gout diagnosis provides support to the idea that bacteria play a protective role in uric acid homeostasis. However, our inclusion criteria were very broad, with patients differing by age, sex, diagnosis, drug doses, and durations. Despite these broad inclusion criteria, patients who received clindamycin carried higher risk for gout, which became more significant after propensity score matching. In this sense, this finding is robust because it is generalizable to a broad population of patients. Nevertheless, it will be important to independently test and validate these findings in different populations and with more strictly defined inclusion criteria.

STAR★METHODS

Detailed methods are provided in the online version of this paper and include the following:

- KEY RESOURCES TABLE
- RESOURCE AVAILABILITY
  - Lead contact
  - Materials availability
  - Data and code availability
- EXPERIMENTAL MODEL AND STUDY PARTICIPANT DETAILS
  - Bacterial strain construction
  - Mouse studies
- METHOD DETAILS
  - Reagents used in this study
  - Bacterial strains and culture conditions
  - Culture conditions for uric acid consumption assays
  - Stable isotope tracing with $^{13}C_5$ labeled uric acid
  - Sample preparation for analysis of uric acid, xanthine, and creatinine by liquid chromatography – mass spectrometry (LC-MS)
  - Sample preparation for analysis of short chain fatty acids by LC-MS
  - 3-Nitrophenylhydrazine (NPH) derivatization protocol
  - Quantification of metabolites by liquid chromatography-mass spectrometry (LC-MS)
  - RNA purification for RNA-seq experiment
  - RNA-seq library preparation and data collection
  - RNA-seq data analysis
  - RNA purification for RT-qPCR
  - Stable isotope tracing in Uox mouse cecal contents

- Metagenomic analysis of uric acid genes in cecal contents of Uox mice
- Impact of antibiotic treatment on risk for Gout diagnosis
- Propensity score model
- Metagenomic analysis of uric acid gene cluster abundances in the FARMM study
- QUANTIFICATION AND STATISTICAL ANALYSIS

SUPPLEMENTAL INFORMATION

Supplemental information can be found online at https://doi.org/10.1016/j.cell.2023.06.010.

AUTHOR CONTRIBUTIONS

Y.L., J.B.J., and D.D. conceived and designed the project; Y.L. and J.B.J. conducted and analyzed uric acid screening assays with help from H.C., D.D., and B.-H.H.; Y.L. performed *in vitro* uric acid consumption assays and stable isotope tracing with help from D.D.; J.B.J. performed RNA-seq experiments and analyzed data with help from D.D.; J.B.J. created bacterial mutants with help from Y.L., K.S., and D.D.; H.C. developed LC-MS assays and analyzed LC-MS data with help from Y.L., J.B.J., and D.D.; Y.L. prepared samples for LC-MS analysis; S.H. and D.D. conducted phylogenetic analyses; Y.L. performed RT-qPCR experiments; M.E.D. assisted with breeding of Uox-deficient mice; Y.L. conducted mouse experiments with help from M.E.D., K.S., and D.D.; A.M.W. and A.V.C. performed metagenomics sequencing; X.M. performed reads pre-processing; Z.Z. and D.D. performed metagenome assemblies, gene cluster searches, and metagenomic read mapping; H.E.A. conducted the FARMM metagenomics analysis, supervised by G.v.W. and M.H.M.; A.C.P., C.G., D.D., S.G., and Y.S.L. conceived and designed the gout cohort analysis; Y.S.L. conducted cohort analysis, advised by S.G.; Y.L. and D.D. wrote the manuscript with input from all co-authors; Y.L. and D.D. prepared all figures with help from S.H., H.E.A., S.G., and Y.S.L.

DECLARATION OF INTERESTS

D.D. is a co-founder of Federation Bio. M.H.M. is a member of the Scientific Advisory Board of Hexagon Bio and co-founder of Design Pharmaceuticals.

INCLUSION AND DIVERSITY

We support inclusive, diverse, and equitable conduct of research.

REFERENCES

1. Kratzer, J.T., Lanaspa, M.A., Murphy, M.N., Cicerchi, C., Graves, C.L., Tipton, P.A., Ortlund, E.A., Johnson, R.J., and Gaucher, E.A. (2014). Evolutionary history and metabolic insights of ancient mammalian uricases. Proc. Natl. Acad. Sci. USA *111*, 3763–3768. https://doi.org/10.1073/pnas.1320393111.

2. Chang, B.S. (2014). Ancient insights into uric acid metabolism in primates. Proc. Natl. Acad. Sci. USA *111*, 3657–3658. https://doi.org/10.1073/pnas.1401037111.

3. Johnson, R.J., Titte, S., Cade, J.R., Rideout, B.A., and Oliver, W.J. (2005). Uric acid, evolution and primitive cultures. Semin. Nephrol. *25*, 3–8. https://doi.org/10.1016/j.semnephrol.2004.09.002.

4. Singh, G., Lingala, B., and Mithal, A. (2019). Gout and hyperuricaemia in the USA: prevalence and trends. Rheumatol. Oxf. Engl. *58*, 2177–2180. https://doi.org/10.1093/rheumatology/kez196.

5. Sorensen, L.B. (1965). Role of the intestinal tract in the elimination of uric acid. Arthritis Rheum. *8*, 694–706. https://doi.org/10.1002/art.1780080429.

6. Hoque, K.M., Dixon, E.E., Lewis, R.M., Allan, J., Gamble, G.D., Phipps-Green, A.J., Halperin Kuhns, V.L., Horne, A.M., Stamp, L.K., Merriman, T.R., et al. (2020). The ABCG2 Q141K hyperuricemia and gout associated variant illuminates the physiology of human urate excretion. Nat. Commun. *11*, 2767. https://doi.org/10.1038/s41467-020-16525-w.

7. Tin, A., Marten, J., Halperin Kuhns, V.L., Li, Y., Wuttke, M., Kirsten, H., Sieber, K.B., Qiu, C., Gorski, M., Yu, Z., et al. (2019). Target genes, variants, tissues and transcriptional pathways influencing human serum urate levels. Nat. Genet. *51*, 1459–1474. https://doi.org/10.1038/s41588-019-0504-x.

8. Kottgen, A., Albrecht, E., Teumer, A., Vitart, V., Krumsiek, J., Hundertmark, C., Pistis, G., Ruggiero, D., O'Seaghdha, C.M., Haller, T., et al. (2013). Genome-wide association analyses identify 18 new loci associated with serum urate concentrations. Nat. Genet. *45*, 145–154. https://doi.org/10.1038/ng.2500.

9. Ermer, T., Nazzal, L., Tio, M.C., Waikar, S., Aronson, P.S., and Knauf, F. (2023). Oxalate homeostasis. Nat. Rev. Nephrol. *19*, 123–138. https://doi.org/10.1038/s41581-022-00643-3.

10. Daniel, S.L., Moradi, L., Paiste, H., Wood, K.D., Assimos, D.G., Holmes, R.P., Nazzal, L., Hatch, M., and Knight, J. (2021). Forty years of *Oxalobacter formigenes*, a gutsy oxalate-degrading specialist. Appl. Environ. Microbiol. *87*, e0054421. https://doi.org/10.1128/AEM.00544-21.

11. Rabinowitz, J.C., and Barker, H.A. (1956). Purine fermentation by *Clostridium cylindrosporum*. I. Tracer experiments on the fermentation of guanine. J. Biol. Chem. *218*, 147–160.

12. Rabinowitz, J.C., and Barker, H.A. (1956). Purine fermentation by *Clostridium cylindrosporum*. II. Purine transformations. J. Biol. Chem. *218*, 161–173.

13. Rabinowitz, J.C. (1956). Purine fermentation by *Clostridium cylindrosporum*. I. Tracer experiments on the fermentation of guanine. J. Biol. Chem. *218*, 175–187.

14. Rabinowitz, J.C., and Pricer, W.E., Jr. (1956). Purine fermentation by *Clostridium cylindrosporum*. IV. 4-Ureido-5-imidazolecarboxylic acid. J. Biol. Chem. *218*, 189–199.

15. Pricer, W.E., Jr., and Rabinowitz, J.C. (1956). Purine fermentation by *Clostridium cylindrosporum*. V. Formiminoglycine. J. Biol. Chem. *222*, 537–554.

16. Poehlein, A., Bengelsdorf, F.R., Schiel-Bengelsdorf, B., Daniel, R., and Dürre, P. (2015). Draft genome sequence of purine-degrading *Gottschalkia purinilyticum* (formerly *Clostridium purinilyticum*) WA1 (DSM 1384). Genome Announc. *3*. https://doi.org/10.1128/genomeA.01088-15.

17. Poehlein, A., Montoya Solano, J.D., Bengelsdorf, F.R., Schiel-Bengelsdorf, B., Daniel, R., and Dürre, P. (2015). Draft genome sequence of purine-degrading *Clostridium cylindrosporum* HC-1 (DSM 605). Genome Announc. *3*. https://doi.org/10.1128/genomeA.00917-15.

18. Hartwich, K., Poehlein, A., and Daniel, R. (2012). The purine-utilizing bacterium *Clostridium acidurici* 9a: a genome-guided metabolic reconsideration. PLoS One *7*, e51662. https://doi.org/10.1371/journal.pone.0051662.

19. Dürre, P., and Andreesen, J.R. (1983). Purine and glycine metabolism by purinolytic clostridia. J. Bacteriol. *154*, 192–199. https://doi.org/10.1128/jb.154.1.192-199.1983.

20. Iwadate, Y., and Kato, J.I. (2019). Identification of a formate-dependent uric acid degradation pathway in *Escherichia coli*. J. Bacteriol. *201*. https://doi.org/10.1128/JB.00573-18.

21. Lu, J., Dalbeth, N., Yin, H., Li, C., Merriman, T.R., and Wei, W.H. (2019). Mouse models for human hyperuricaemia: a critical review. Nat. Rev. Rheumatol. *15*, 413–426. https://doi.org/10.1038/s41584-019-0222-x.

22. Wu, X., Wakamiya, M., Vaishnav, S., Geske, R., Montgomery, C., Jr., Jones, P., Bradley, A., and Caskey, C.T. (1994). Hyperuricemia and urate nephropathy in urate oxidase-deficient mice. Proc. Natl. Acad. Sci. USA *91*, 742–746. https://doi.org/10.1073/pnas.91.2.742.

23. Watanabe, T., Tomioka, N.H., Watanabe, S., Tsuchiya, M., and Hosoyamada, M. (2014). False *in vitro* and *in vivo* elevations of uric acid levels in mouse blood. Nucleosides Nucleotides Nucleic Acids *33*, 192–198. https://doi.org/10.1080/15257770.2013.865742.

24. Mazzali, M., Hughes, J., Kim, Y.G., Jefferson, J.A., Kang, D.H., Gordon, K.L., Lan, H.Y., Kivlighn, S., and Johnson, R.J. (2001). Elevated uric acid increases blood pressure in the rat by a novel crystal-independent mechanism. Hypertension *38*, 1101–1106. https://doi.org/10.1161/hy1101.092839.

25. Tanes, C., Bittinger, K., Gao, Y., Friedman, E.S., Nessel, L., Paladhi, U.R., Chau, L., Panfen, E., Fischbach, M.A., Braun, J., et al. (2021). Role of dietary fiber in the recovery of the human gut microbiome and its metabolome. Cell Host Microbe *29*, 394–407.e5. https://doi.org/10.1016/j.chom.2020.12.012.

26. Pascal Andreu, V., Roel-Touris, J., Dodd, D., Fischbach, M.A., and Medema, M.H. (2021). The gutSMASH web server: automated identification of primary metabolic gene clusters from the gut microbiota. Nucleic Acids Res. *49*, W263–W270. https://doi.org/10.1093/nar/gkab353.

27. Pascal Andreu, V., Augustijn, H.E., Chen, L., Zhernakova, A., Fu, J., Fischbach, M.A., Dodd, D., and Medema, M.H. (2023). gutSMASH predicts specialized primary metabolic pathways from the human gut microbiota. Nat. Biotechnol. https://doi.org/10.1038/s41587-023-01675-1.

28. Pascal Andreu, V., Augustijn, H.E., van den Berg, K., van der Hooft, J.J.J., Fischbach, M.A., and Medema, M.H. (2021). BiG-MAP: an automated pipeline to profile metabolic gene cluster abundance and expression in microbiomes. mSystems *6*, e0093721. https://doi.org/10.1128/mSystems.00937-21.

29. Barsoum, R., and El-Khatib, M. (2017). Uric acid and life on earth. J. Adv. Res. *8*, 471–474. https://doi.org/10.1016/j.jare.2017.06.001.

30. Vogels, G.D., and Van der Drift, C. (1976). Degradation of purines and pyrimidines by microorganisms. Bacteriol. Rev. *40*, 403–468. https://doi.org/10.1128/br.40.2.403-468.1976.

31. Kasahara, K., Kerby, R.L., Zhang, Q., Pradhan, M., Mehrabian, M., Lusis, A.J., Bergström, G., Bäckhed, F., and Rey, F.E. (2023). Gut bacterial metabolism contributes to host global purine homeostasis. Cell Host Microbe *31*, 1038–1053.e10. https://doi.org/10.1016/j.chom.2023.05.011.

32. Johnson, R.J., Sánchez-Lozada, L.G., Nakagawa, T., Rodriguez-Iturbe, B., Tolan, D., Gaucher, E.A., Andrews, P., and Lanaspa, M.A. (2022). Do thrifty genes exist? Revisiting uricase. Obesity (Silver Spring) *30*, 1917–1926. https://doi.org/10.1002/oby.23540.

33. Pierzynowska, K., Deshpande, A., Mosiichuk, N., Terkeltaub, R., Szczurek, P., Salido, E., Pierzynowski, S., and Grujic, D. (2020). Oral treatment with an engineered uricase, ALLN-346, reduces hyperuricemia, and uricosuria in urate oxidase-deficient mice. Front. Med. (Lausanne) *7*, 569215. https://doi.org/10.3389/fmed.2020.569215.

34. Terkeltaub, R., Clark, D., Tosone, C., Kandinov, B., Zhang, P., Dahl, N., Grujic, D., and Goldfarb, D. (2022). POS1157 Safety and efficacy of ALLN-346 oral enzyme therapy in patients with hyperuricemia and chronic kidney disease (CKD): results of the phase 2A study 201. Ann. Rheum. Dis. 81, 907–921. https://doi.org/10.1136/annrheumdis-2022-eular.1662.

35. Mandal, A.K., and Mount, D.B. (2015). The molecular physiology of uric acid homeostasis. Annu. Rev. Physiol. 77, 323–345. https://doi.org/10.1146/annurev-physiol-021113-170343.

36. Heap, J.T., Kuehne, S.A., Ehsaan, M., Cartman, S.T., Cooksley, C.M., Scott, J.C., and Minton, N.P. (2010). The ClosTron: mutagenesis in Clostridium refined and streamlined. J. Microbiol. Methods 80, 49–55. https://doi.org/10.1016/j.mimet.2009.10.018.

37. Dodd, D., Spitzer, M.H., Van Treuren, W., Merrill, B.D., Hryckowian, A.J., Higginbottom, S.K., Le, A., Cowan, T.M., Nolan, G.P., Fischbach, M.A., et al. (2017). A gut bacterial pathway metabolizes aromatic amino acids into nine circulating metabolites. Nature 551, 648–652. https://doi.org/10.1038/nature24661.

38. Liu, Y., Chen, H., Van Treuren, W., Hou, B.H., Higginbottom, S.K., and Dodd, D. (2022). Clostridium sporogenes uses reductive Stickland metabolism in the gut to generate ATP and produce circulating metabolites. Nat. Microbiol. 7, 695–706. https://doi.org/10.1038/s41564-022-01109-9.

39. Datsenko, K.A., and Wanner, B.L. (2000). One-step inactivation of chromosomal genes in Escherichia coli K-12 using PCR products. Proc. Natl. Acad. Sci. USA 97, 6640–6645. https://doi.org/10.1073/pnas.120163297.

40. Thomason, L.C., Costantino, N., and Court, D.L. (2007). E. coli genome manipulation by P1 transduction. Curr. Protoc. Mol. Biol., 1.17.1–1.17.8. https://doi.org/10.1002/0471142727.mb0117s79.

41. Ray, W.A. (2003). Evaluating medication effects outside of clinical trials: new-user designs. Am. J. Epidemiol. 158, 915–920. https://doi.org/10.1093/aje/kwg231.

42. Quan, H., Sundararajan, V., Halfon, P., Fong, A., Burnand, B., Luthi, J.C., Saunders, L.D., Beck, C.A., Feasby, T.E., and Ghali, W.A. (2005). Coding algorithms for defining comorbidities in ICD-9-CM and ICD-10 administrative data. Med. Care 43, 1130–1139. https://doi.org/10.1097/01.mlr.0000182534.19832.83.

43. Austin, P.C. (2011). An introduction to propensity score methods for reducing the effects of confounding in observational studies. Multivariate Behav. Res. 46, 399–424. https://doi.org/10.1080/00273171.2011.568786.

44. Schneeweiss, S., Rassen, J.A., Glynn, R.J., Avorn, J., Mogun, H., and Brookhart, M.A. (2009). High-dimensional propensity score adjustment in studies of treatment effects using health care claims data. Epidemiology 20, 512–522. https://doi.org/10.1097/EDE.0b013e3181a663cc.

45. Franklin, J.M., Eddings, W., Glynn, R.J., and Schneeweiss, S. (2015). Regularized regression versus the high-dimensional propensity score for confounding adjustment in secondary database analyses. Am. J. Epidemiol. 182, 651–659. https://doi.org/10.1093/aje/kwv108.

46. Low, Y.S., Gallego, B., and Shah, N.H. (2016). Comparing high-dimensional confounder control methods for rapid cohort studies from electronic health records. J. Comp. Eff. Res. 5, 179–192. https://doi.org/10.2217/cer.15.53.

47. Hastie, T., Tibshirani, R., and Friedman, J. (2009). The Elements of Statistical Learning: Data Mining, Inference, and Prediction, Second Edition (Springer). https://doi.org/10.1007/978-0-387-84858-7.

48. Callahan, A., Gombar, S., Cahan, E.M., Jung, K., Steinberg, E., Polony, V., Morse, K., Tibshirani, R., Hastie, T., Harrington, R., et al. (2021). Using aggregate patient data at the bedside via an on-demand consultation service. NEJM Catal. 2. https://doi.org/10.1056/CAT.21.0224.

49. Edgar, R.C. (2004). MUSCLE: a multiple sequence alignment method with reduced time and space complexity. BMC Bioinformatics 5, 113. https://doi.org/10.1186/1471-2105-5-113.

50. Paulson, J.N., Stine, O.C., Bravo, H.C., and Pop, M. (2013). Differential abundance analysis for microbial marker-gene surveys. Nat. Methods 10, 1200–1202. https://doi.org/10.1038/nmeth.2658.

51. Gu, Z., Eils, R., and Schlesner, M. (2016). Complex heatmaps reveal patterns and correlations in multidimensional genomic data. Bioinformatics 32, 2847–2849. https://doi.org/10.1093/bioinformatics/btw313.

52. Wickham, H. (2009). ggplot2: Elegant Graphics for Data Analysis (Springer). https://doi.org/10.1007/978-0-387-98141-3.

STAR★METHODS

KEY RESOURCES TABLE

REAGENT or RESOURCE	SOURCE	IDENTIFIER
Bacterial and virus strains		
Wild-type gut bacterial strains used in this study	See Table S4	See Table S4
E. coli Stbl4 ElectroMax	Invitrogen	11635018
Chemicals, peptides, and recombinant proteins		
3-nitrophenylhydrazine hydrochloride	Sigma Aldrich	N21804
acetic acid	Sigma Aldrich	6283
acetic acid-d4, ≥99.9 atom % D	Sigma Aldrich	233315
acetonitrile	Fisher Scientific	A955-4
allopurinol	Sigma Aldrich	A8003
ammonium acetate	Fisher Scientific	A11450
ammonium hydroxide solution	Honeywell Fluka	4427310X1ML
butyric acid	Sigma Aldrich	B103500
calcium chloride	Alfa Aesar	89866
chloramphenicol	Sigma Aldrich	C1919
chopped meat medium	Anaerobe Systems	AS-811
creatinine	Sigma Aldrich	C4255
creatinine (*N*-methyl-D3, 98%)	Cambridge Isotope Laboratories	DLM-3653
D(-)-fructose	Sigma Aldrich	F0127
D(+)-cellobiose	Fluka Chemie GMBH	22150
D(+)-maltose, monohydrate	Acros	329915000
dansyl chloride	Sigma Aldrich	D2625
D-cycloserine	Sigma Aldrich	C6880
dextrose (D-glucose), anhydrous	Fisher Scientific	D16-500
Difco Brain Heart Infusion Broth	BD	237500
Difco Brain Heart Infusion Agar	BD	241810
Difco LB Broth, Miller (Luria-Bertani)	BD	244610
Difco Reinforced Clostridial Medium (RCM)	BD	218081
dimethyl sulfoxide	MP Biomedicals	219605590
erythromycin	Sigma Aldrich	E5389
ethanol	Fisher Scientific	BP2818
ferrous sulfate heptahydrate	Fisher Scientific	I146
formic acid	Fisher Scientific	A117-50
GAM Agar	Nissui	05420
GAM Broth	Nissui	05422
GAM Broth, Modified	Nissui	05433
glycerol	Fisher Scientific	BP229-1
glycine	Sigma Aldrich	G7126
hematin, porcine	Sigma Aldrich	H3281
hydrochloric acid	Fisher Scientific	SA49
hydrocinnamic acid-d9 (phenylpropionic acid-d9)	C/D/N Isotopes	D-5666
isobutyric acid	Sigma Aldrich	58360
isovaleric acid	Sigma Aldrich	129542
lactic acid	Fisher Chemical	A159-500
L-cysteine hydrochloride monohydrate	Sigma Aldrich	C7880
L-histidine	Sigma Aldrich	H8000

(Continued on next page)

Continued

REAGENT or RESOURCE	SOURCE	IDENTIFIER
M9 Minimal Salts, 5x	BD	248510
magnesium sulfate heptahydrate	Fisher Scientific	M63-500
meat extract	Sigma Aldrich	70164
menadione	Sigma Aldrich	M5625
methanol	Fisher Scientific	A456-4
mucin type III	Sigma Aldrich	M1778
N-(3-dimethylaminopropyl)-*N'*-ethylcarbodiimide	Sigma Aldrich	3449
n-butyric acid	Sigma Aldrich	B103500
potassium oxonate	Ambeed	A157215
potassium phosphate dibasic	Fisher Scientific	BP363
potassium phosphate monobasic	Fisher Scientific	BP362
propionic acid	Sigma Aldrich	402907
pyridine	Sigma Aldrich	270970
resazurin, sodium salt	Acros	418900050
sodium acetate	Sigma Aldrich	S2889
sodium bicarbonate	Fisher Scientific	S233-500
sodium butyrate	Sigma Aldrich	303410
sodium carbonate	Fisher Scientific	S263-500
sodium chloride	Fisher Scientific	S271-500
sodium fumarate dibasic	Sigma Aldrich	F1506
sodium hydroxide	Fisher Scientific	S318-500
sodium phosphate, dibasic, anhydrous	Caisson Labs	S018-500GM
sodium propionate	Sigma Aldrich	P1880
sodium thioglycolate	BD	B12081
sterilized rumen fluid	Bar Diamond Inc.	SRF
succinic acid	Tokyo Chemical Industry (TCI)	S0100
thiamphenicol	Sigma Aldrich	T0261
trace mineral supplement	ATCC	MD-TMS
tryptone	BD	211705
tryticase peptone, pancreatic digest of casein	BD	221921
tween 80	Fisher Scientific	T164-500
uric acid	Sigma Aldrich	U2625
uric acid (1,3-15N2, 98%+)	Cambridge Isotope Laboratories	NLM-1697-PK
uric acid (13C5, 99.3%)	Acanthus Research	U-10826-01
valeric acid	Sigma Aldrich	240370
vitamin K_1	Sigma Aldrich	V3501
vitamin supplement	ATCC	MD-VS
water	Fisher Scientific	W6-4
xanthine	Tokyo Chemical Industry (TCI)	X0004
xanthine (1,3-15N2, 98%+) 90% PURE	Cambridge Isotope Laboratories	NLM-1698-PK
yeast extract	BD	288620
Medium formulations	See Table S4	See Table S4
Critical commercial assays		
AcroPrep Advance Filter Plates for Ultrafiltration with Omega Membrane, MWCO 3K	Pall Corporation	8033
DNA Clean & Concentrator-5, Capped Columns	Zymo Research	D4013

Continued

REAGENT or RESOURCE	SOURCE	IDENTIFIER
RNAprotect Bacteria Reagent	Qiagen	76506
PowerUp SYBR Green Master Mix	ThermoFisher	A25778
PrimeSTAR Max DNA Polymerase	Takara	R045A
Qubit RNA BR assay kit	ThermoFisher	Q10210
SuperScript IV VILO Master Mix with ezDNase Enzyme	ThermoFisher	11766050
Terra PCR Direct Genotyping Kit	Takara	639285
Urea Assay Kit	Sigma Aldrich	MAK006
Deposited data		
RNA-seq data	NCBI Gene Expression Omnibus	GEO: GSE206419
Metagenomic reads from *Uox* mice	NCBI BioProject	PRJNA947216
Metagenomic data re-analyzed from the FARMM study	NCBI BioProject	PRJNA675301
Metabolomics data re-analyzed from the FARMM study	Metabolomics Workbench	Study ID ST001519
Reference genomes analyzed from the Human Microbiome Project	NCBI BioProject	PRJNA43021
Custom R script for the metagenomic data processing and figure generation	Github	https://github.com/HAugustijn/uric_acid_project/
Experimental models: Organisms/strains		
Uricase deficient mice (B6; 129S7-Uox^tm1Bay/J)	The Jackson Laboratory	002223; RRID:IMSR_JAX:002223
Germ-free C57BL/6 mice (C57BL/6NTac)	Taconic Biosciences	www.taconic.com
C. sporogenes ATCC 15579; wild-type	ATCC	www.atcc.org
C. sporogenes ATCC 15579; *ygeX*(1026a)::CT	This study	N/A
C. sporogenes ATCC 15579; *pbuX*(952a)::CT	This study	N/A
C. sporogenes ATCC 15579; *hyuA*(524a)::CT	This study	N/A
C. sporogenes ATCC 15579; *ygeW*(1034a)::CT	This study	N/A
C. sporogenes ATCC 15579; *ygfK*(1440a)::CT	This study	N/A
C. sporogenes ATCC 15579; *ssnA*(784s)::CT	This study	N/A
C. sporogenes ATCC 15579; *ygeY*(358s)::CT	This study	N/A
C. sporogenes ATCC 15579; *xdhAC*(1084s)::CT	This study	N/A
E. coli MG 1655; wild-type	*E. coli* Genetic Stock Center	www.cgsc.biology.yale.edu
E. coli MG 1655; Δ(*ygeW::cat*)1	This study	N/A
E. coli MG 1655; Δ(*ygeX::cat*)1	This study	N/A
E. coli MG 1655; Δ(*ygeY::cat*)1	This study	N/A
E. coli MG 1655; Δ(*hyuA::cat*)1	This study	N/A
E. coli MG 1655; Δ(*ygfK::cat*)1	This study	N/A
E. coli MG 1655; Δ(*ssnA::cat*)1	This study	N/A
Oligonucleotides		
ygeX (CLOSPO_02124, 1026a) gBlock: ATAAAGTTGTGTAATTTTTAAGCTTTATAATTATCCTTAGACTCCCCTGATGTGCGCCCAGATAGGGTGTTAAGTCAAGTAGTTTAAGGTACTACTCTGTAAGATAACACAGAAAACAGCCAACCTAACCGAAAAGCGAAAGCTGATACGGGAACAGAGCACGGTTGGAAAGCGATGAGTTACCTAAAGACAATCGGGTACGACTGAGTCGCAATGTTAATCAGATATAAGGTATAAGTTGTGTTTACTGAACGCAAGTTTCTAATTTCGATTGAGTCTCGATAGAGGAAAGTGTCTGAAACCTCTAGTACAAAGAAAGGTAAGTTAATATCAGGGACTTATCTGTTATCACCACATTTGTACAATCTGTAGGAGAACCTATGG	Integrated DNA technologies	N/A
pbuX (CLOSPO_02125, 952s) gBlock: ATAAAGTTGTGTAATTTTTAAGCTTTATAATTATCCTTACAAAACGTAGGGGGTGCGCCCAGATAGGGTGTTAAGTCAAGTAGTTTAAGGTA	Integrated DNA technologies	N/A

Continued

REAGENT or RESOURCE	SOURCE	IDENTIFIER
CTACTCTGTAAGATAACACAGAAAACAGCCAACCTAACCGAAA AGCGAAAGCTGATACGGGAACAGAGCACGGTTGGAAAGCGA TGAGTTACCTAAAGACAATCGGGTACGACTGAGTCGCAATGTT AATCAGATATAAGGTATAAGTTGTGTTTACTGAACGCAAGTTTC TAATTTCGGTTTTTTGTCGATAGAGGAAAGTGTCTGAAACCTCT AGTACAAAGAAAGGTAAGTTAAGCCCTACGACTTATCTGTTAT CACCACATTTGTACAATCTGTAGGAGAACCTATGG		
hyuA (CLOSPO_02126, 524a) gBlock: ATAAAGTTGTGTAATTTTTAAGCTTTATAATTATCCTTACTGTAC GTATACGTGCGCCCAGATAGGGTGTTAAGTCAAGTAGTTTAA GGTACTACTCTGTAAGATAACACAGAAAACAGCCAACCTAAC CGAAAAGCGAAAGCTGATACGGGAACAGAGCACGGTTGGAA AGCGATGAGTTACCTAAAGACAATCGGGTACGACTGAGTCGC AATGTTAATCAGATATAAGGTATAAGTTGTGTTTACTGAACGC AAGTTTCTAATTTCGGTTTACAGTCGATAGAGGAAAGTGTCTG AAACCTCTAGTACAAAGAAAGGTAAGTTATGGTATACGACTTA TCTGTTATCACCACATTTGTACAATCTGTAGGAGAACCTATGG	Integrated DNA technologies	N/A
ygeW (CLOSPO_02127, 1034a) gBlock: ATAAAGTTGTGTAATTTTTAAGCTTTATAATTATCCTTACTGATC CAGCTAGTGCGCCCAGATAGGGTGTTAAGTCAAGTAGTTTAA GGTACTACTCTGTAAGATAACACAGAAAACAGCCAACCTAAC CGAAAAGCGAAAGCTGATACGGGAACAGAGCACGGTTGGAA AGCGATGAGTTACCTAAAGACAATCGGGTACGACTGAGTCGC AATGTTAATCAGATATAAGGTATAAGTTGTGTTTACTGAACGC AAGTTTCTAATTTCGGTTATCAGTCGATAGAGGAAAGTGTCTG AAACCTCTAGTACAAAGAAAGGTAAGTTAGGTAGCTGGACTTA TCTGTTATCACCACATTTGTACAATCTGTAGGAGAACCTATGG	Integrated DNA technologies	N/A
ygfK (CLOSPO_02128, 1440a) gBlock: ATAAAGTTGTGTAATTTTTAAGCTTTATAATTATCCTTAGTATTC TCCTTAGTGCGCCCAGATAGGGTGTTAAGTCAAGTAGTTTAAG GTACTACTCTGTAAGATAACACAGAAAACAGCCAACCTAACCG AAAAGCGAAAGCTGATACGGGAACAGAGCACGGTTGGAAAGC GATGAGTTACCTAAAGACAATCGGGTACGACTGAGTCGCAATG TTAATCAGATATAAGGTATAAGTTGTGTTTACTGAACGCAAGTT TCTAATTTCGATTAATACTCGATAGAGGAAAGTGTCTGAAACCT CTAGTACAAAGAAAGGTAAGTTAGCTAAGGAGACTTATCTGTT ATCACCACATTTGTACAATCTGTAGGAGAACCTATGG	Integrated DNA technologies	N/A
ssnA (CLOSPO_02129, 784s) gBlock: ATAAAGTTGTGTAATTTTTAAGCTTTATAATTATCCTTAATAGCC GTACATGTGCGCCCAGATAGGGTGTTAAGTCAAGTAGTTTAAG GTACTACTCTGTAAGATAACACAGAAAACAGCCAACCTAACCG AAAAGCGAAAGCTGATACGGGAACAGAGCACGGTTGGAAAGC GATGAGTTACCTAAAGACAATCGGGTACGACTGAGTCGCAAT GTTAATCAGATATAAGGTATAAGTTGTGTTTACTGAACGCAAG TTTCTAATTTCGGTTGCTATCCGATAGAGGAAAGTGTCTGAAA CCTCTAGTACAAAGAAAGGTAAGTTACAATGTACGACTTATCT GTTATCACCACATTTGTACAATCTGTAGGAGAACCTATGG	Integrated DNA technologies	N/A
ygeY (CLOSPO_02130, 358s) gBlock: ATAAAGTTGTGTAATTTTTAAGCTTTATAATTATCCTTAGGCGG CATGGCCGTGCGCCCAGATAGGGTGTTAAGTCAAGTAGTTTA AGGTACTACTCTGTAAGATAACACAGAAAACAGCCAACCTAA CCGAAAAGCGAAAGCTGATACGGGAACAGAGCACGGTTGGA AAGCGATGAGTTACCTAAAGACAATCGGGTACGACTGAGTCG CAATGTTAATCAGATATAAGGTATAAGTTGTGTTTACTGAACG CAAGTTTCTAATTTCGATTCCGCCTCGATAGAGGAAAGTGTC TGAAACCTCTAGTACAAAGAAAGGTAAGTTAGAGGCCATGAC TTATCTGTTATCACCACATTTGTACAATCTGTAGGAGAACCT ATGG	Integrated DNA technologies	N/A

Continued

REGENT or RESOURCE	SOURCE	IDENTIFIER
xdhAC (CLOSPO_02131, 1084s) gBlock: ATAAAGTTGTGTAATTTTTAAGCTTTATAATTATCCTTAGATGGCG ATGGAGTGCGCCCAGATAGGGTGTTAAGTCAAGTAGTTTAAGG TACTACTCTGTAAGATAACACAGAAAACAGCCAACCTAACCGAA AAGCGAAAGCTGATACGGGAACAGAGCACGGTTGGAAAGCGA TGAGTTACCTAAAGACAATCGGGTACGACTGAGTCGCAATGTT AATCAGATATAAGGTATAAGTTGTGTTTACTGAACGCAAGTTTC TAATTTCGATTCCATCTCGATAGAGGAAAGTGTCTGAAACCTCT AGTACAAAGAAAGGTAAGTTAACTCCATCGACTTATCTGTTATC ACCACATTTGTACAATCTGTAGGAGAACCTATGG	Integrated DNA technologies	N/A
ygeX (CLOSPO_02124) sequencing Csp.ygeX-F: AGTAACTGGAGATATGCCTA Csp.ygeX-R: TACTAAAGTTGCTATGCCT	Integrated DNA technologies	N/A
pbuX (CLOSPO_02125) sequencing Csp.pbuX-F: TTTTGTTTTATTATGGCACCT Csp.pbuX-R: TGCCAAACATAGCTATACCA	Integrated DNA technologies	N/A
hyuA (CLOSPO_02126) sequencing Csp.hyuA-F: AAATCATTGATGCTCATGG Csp.hyuA-R: TAATCTAACCCTAACTTACAGG	Integrated DNA technologies	N/A
ygeW (CLOSPO_02127) sequencing Csp.ygeW-F: CATCTTATGGTAAGCCACT Csp.ygeW-R: GTTCTTCAAACTTTAGGGCTG	Integrated DNA technologies	N/A
ygfK (CLOSPO_02128) sequencing Csp.ygfK-F: CTTCTAAAGGCAAACAAGC Csp.ygfK-R: TAACCTTTCCATTTCCGAT	Integrated DNA technologies	N/A
ssnA (CLOSPO_02129) sequencing Csp.ssnA-F: AAGGAAAACTTATAATGCCAG Csp.ssnA-R: CATTTCAGGAATTTCGGTC	Integrated DNA technologies	N/A
ygeY (CLOSPO_02130) sequencing Csp.ygeY-F: TTTTAAAAGAAGGTGCTCT Csp.ygeY-R: TTCATACACATTTATTACCCC	Integrated DNA technologies	N/A
xdhAC (CLOSPO_02131) sequencing Csp.xdhAC-F: ATTATTACAGCACAAGATGTCC Csp.xdhAC-R: CGCATGATGTTGTACACTCA	Integrated DNA technologies	N/A
ygeW (b2870) λ-red recombination knockout F: TTTGCCTGTCATTCCACTACCGGGACTTTATGATGGTGTAGGC TGGAGCTGCTTC R: ATCGGCCCGAGGGGTTATTTCACGCGTTCTTGCGCCCATATG AATATCCTCCTTAGT	Integrated DNA technologies	N/A
ygeX (b2871) λ-red recombination knockout F: CCCTCTATTTCCAGAGGCCAAAAGGATAGGATATGGTGTAGG CTGGAGCTGCTTC R: TTCCAATAGGGTGATTAAGGTGCTACAGCGTGTTTCCATATG AATATCCTCCTTAGT	Integrated DNA technologies	N/A
ygeY (b2872) λ-red recombination knockout F: AAAACGGGGAGTAAAAAATCTGGAGAAAAATAATGGTGTAGG CTGGAGCTGCTTC R: GCCCATGATAGATACGCCGTTAGTTGAGAAGGTCCCCATAT GAATATCCTCCTTAGT	Integrated DNA technologies	N/A
hyuA (b2873) λ-red recombination knockout F: TCCGGTTCGCCGGAGGGTTTTTGGAGTTTGCTATGGTGTAG GCTGGAGCTGCTTC R: ATCCCTGGCAGTGGTTAGAGCACGGGAGGGACAAACCATAT GAATATCCTCCTTAGT	Integrated DNA technologies	N/A
ygfK (b2878) λ-red recombination knockout F: CAATGATATCTGTATAAGCTAAGGAGAGGGTTATGGTGTAGG	Integrated DNA technologies	N/A

Continued

REAGENT or RESOURCE	SOURCE	IDENTIFIER
CTGGAGCTGCTTC R: CGCCAGGCTGAAGACGGTGATTTTGTCTTTGTACGCCATAT GAATATCCTCCTTAGT		
ssnA (b2879) λ-red recombination knockout F: CATTATCTGCTGGGCCGCGTGGAGGTGTAATCATGGTGTAG GCTGGAGCTGCTTC R: AGGGCATCTGTCATTTATGCCAGCGCATCCATCCGCCATA TGAATATCCTCCTTAGT	Integrated DNA technologies	N/A
ygeW (b2870) sequencing Ec.ygeW-CHF: GAATTTGCATCAATACTGACTG Ec.ygeW-CHR: TAACCTTCCCATGCCGTGTC	Integrated DNA technologies	N/A
ygeX (b2871) sequencing Ec.ygeX-CHF: GAGCGTACTGAATTGCTGCG Ec.ygeX-CHR: CGTACGGATCGAAGTCCCAG	Integrated DNA technologies	N/A
ygeY (b2872) sequencing Ec.ygeY-CHF: TGAAGCACTACCGCGAAGTT Ec.ygeY-CHR: TCGTAACTGCGTTCGTCCAA	Integrated DNA technologies	N/A
hyuA (b2873) sequencing Ec.hyuA-CHF: CTGAAGCGCATGCACCTAAC Ec.hyuA-CHR: TCAGTTTTTGCGGCAGCTTC	Integrated DNA technologies	N/A
ygfK (b2878) sequencing Ec.ygfK-CHF: AGGCAATCCAACGACCCAAT Ec.ygfK-CHR: ATCGCGCTGATTGAGTAGGG	Integrated DNA technologies	N/A
ssnA (b2879) sequencing Ec.ssnA-CHF: TCCAGAACCGTTTCCAGACG Ec.ssnA-CHR: AGGCCAGGTAGTCCTCGATT	Integrated DNA technologies	N/A
aegA (b2468) RT-qPCR (Amplification factor 2.07) Ec.aegA-F: AGGTCACTGCACTACGTTGCT Ec.aegA-R: ATGATGAGCAACATGTCCTGAGCC	Integrated DNA technologies	N/A
ygfK (b2878) RT-qPCR (Amplification factor 2.03) Ec.ygfK-F: TTGACGCGCATATTTGATGAATACC Ec.ygfK-R: AGGTTTCACCGAAGACGCTAACA	Integrated DNA technologies	N/A
ygfT (b2887) RT-qPCR (Amplification factor 2.04) Ec.ygfT-F: TCGCATCATCCCGTAAGTCCC Ec.ygfT-R: ATCTTAACTGTGAAATTGGCCGCG	Integrated DNA technologies	N/A
rpoH (b3461) RT-qPCR (Amplification factor 1.98) Ec.rpoH-F: CACTGCTTTCATCAGGCCGA Ec.rpoH-R: AAACGCTGATCCTGTCTCACC	Integrated DNA technologies	N/A
K127_2399939 *ygeX* RT-qPCR (Amplification factor 1.97) YgeX-F: TATTTAGGGCTTGGTGAGGTTTACA YgeX-R: TTTGCTATGTAACGTGCCATGG	Integrated DNA technologies	N/A
K127_2399939 *ygeY* RT-qPCR (Amplification factor 1.96) YgeY-F: TCTGCCGAGTGTTAAGAAATATGGG YgeY-R: TAGCACTCGATAGGATATACCAGGT	Integrated DNA technologies	N/A
K127_2399939 *ssnA* RT-qPCR (Amplification factor 1.94) SsnA-F: TTATGTACTACGCAGGTATCGGT SsnA-R: GGATATTCTGGGACCAAAGACGA	Integrated DNA technologies	N/A
K127_1837117 *ygeX* RT-qPCR (Amplification factor 2.00) YgeX-F: TCTGTTGAGAACATGAGCACA YgeX-R: TCCTTTCCGCCATTATGGAG	Integrated DNA technologies	N/A
K127_1837117 *ygeY* RT-qPCR (Amplification factor 1.95) YgeY-F: AGTGGGTTCAGTGGAGATGAC YgeY-R: ACTGCGACGGTATGTGCTG	Integrated DNA technologies	N/A
K127_1837117 *ssnA* RT-qPCR (Amplification factor 1.91) SsnA-F: CCGTTGATAATAGTAGTGCGGCA SsnA-R: TGATTGTCATGGATTACAAGCCCT	Integrated DNA technologies	N/A

(Continued on next page)

Continued

REAGENT or RESOURCE	SOURCE	IDENTIFIER
K127_2793018 *ygeX* RT-qPCR (Amplification factor 2.00) YgeX-F: AGAAGTCGGTTGTACATATGCCG YgeX-R: CGCCATACGGACACATTCATCA	Integrated DNA technologies	N/A
K127_2793018 *ygeY* RT-qPCR (Amplification factor 1.97) YgeY-F: GTTCGGTGCAGGAGGAAGAC YgeY-R: CGGTCGGTTCGGTCGAAATA	Integrated DNA technologies	N/A
K127_2793018 *ssnA* RT-qPCR (Amplification factor 1.87) SsnA-F: TTCGGCATGATGGGCAAGAA SsnA-R: TGACTGCTCCATCGTCCATG	Integrated DNA technologies	N/A
UOx genotyping oIMR1621: CGAGACCTTTGCAATGAACA oIMR1622: CTCATCTGCTCCACCTCACA oIMR6218: CCTTCTATCGCCTTCTTGACG	The Jackson Laboratory	Protocol 31298
Recombinant DNA		
Plasmid pMTL007C-E2-*ygeX* (CLOSPO_02124); 1026a	This paper	N/A
Plasmid pMTL007C-E2-*pbuX* (CLOSPO_02125); 952s	This paper	N/A
Plasmid pMTL007C-E2-*hyuA* (CLOSPO_02126); 524a	This paper	N/A
Plasmid pMTL007C-E2-*ygeW* (CLOSPO_02127); 1034a	This paper	N/A
Plasmid pMTL007C-E2-*ygfK* (CLOSPO_02128); 1440a	This paper	N/A
Plasmid pMTL007C-E2-*ssnA* (CLOSPO_02129); 784s	This paper	N/A
Plasmid pMTL007C-E2-*ygeY* (CLOSPO_02130); 358s	This paper	N/A
Plasmid pMTL007C-E2-*xdhAC* (CLOSPO_02131); 1084s	This paper	N/A
Software and algorithms		
MassHunter Workstation LC/MS Data Acquisition	Agilent Technologies	v.10.1
MassHunter Workstation Quantitative Analysis	Agilent Technologies	v.10.0
CLC Genomics Workbench	QIAGEN	v.21.0.4
GraphPad Prism	GraphPad Software, LLC	v.9.3.1
QuantStudio 5 qPCR Data Analysis Software	ThermoFisher Scientific	v.1.5.1

RESOURCE AVAILABILITY

Lead contact
Further information and requests for resources and reagents should be directed to and will be fulfilled by the lead contact, Dylan Dodd (ddodd2@stanford.edu).

Materials availability
All unique/stable reagents generated in this study are available from the lead contact without restriction.

Data and code availability
- Data: All metabolite measurements by LC-MS are provided in Table S4. The RNA-seq data has been uploaded to the NCBI Gene Expression Omnibus under accession number GSE206419. Bacterial genome assemblies analyzed in this study (e.g., for phylogenetic trees and BLASTp searches) are from publicly available sources and relevant accession numbers are provided in Table S4. Metagenomic sequence reads from *Uox* mice are deposited at NCBI under BioProject PRJNA947216. Metagenome assembled contigs containing uric acid genes from *Uox* mice are provided in Data S1. Metabolomics and metagenomics data re-analyzed from a study investigating microbiota recovery after depletion[26] was obtained from the Metabolomics Workbench (Study ID ST001519) and NCBI (BioProject PRJNA675301), respectively. Reference genomes of the HMP dataset were obtained from NCBI BioProject PRJNA43021.
- Code: The custom R script for the metagenomic data processing and figure generation can be found at https://github.com/HAugustijn/uric_acid_project/.
- Additional information: Any additional information required to reanalyze the data reported in this paper is available from the lead contact upon request.

EXPERIMENTAL MODEL AND STUDY PARTICIPANT DETAILS

Bacterial strain construction

Gene disruption in Clostridium sporogenes ATCC 15579 using ClosTron

For *Clostridium sporogenes*, gene disruptions were constructed using the Intron targeting and design tool on the ClosTron website (http://www.clostron.com/clostron2.php) with the Perutka algorithm.[37] The intron within the pMTL007C-E2 plasmid was re-targeted to the sites listed in the key resources table and the targeting sequences were synthesized as gBlocks by IDT. Re-targeted plasmids were made by digesting the pMTL007C-E2-CLOSPO_00316-736s[24] plasmid with BsrGI and HindIII, followed by gel-purification of the plasmid backbone and Gibson assembly with re-targeted intron gBlock fragments using the Gibson Assembly Master Mix (NEB). Gibson assemblies were transformed into *E. coli* by electroporation, selected on LB-chloramphenicol (25 μg/mL) plates and sequenced to confirm the correct retargeted sequence. Intron re-targeted plasmids were transformed into *E. coli* S17-1 λpir and subsequently conjugated into *C. sporogenes* as described previously.[38] Mutants were verified by PCR and Sanger sequencing using the sequencing primers listed the key resources table.

Gene disruption in Escherichia coli MG1655 using λ-red recombination

Gene disruption in *Escherichia coli* was first constructed by the λ-red recombination deletion method[39] in BW25113 strain and then was transferred to MG1655 by P1 transduction.[40] The antibiotic resistance cassettes were removed by FLP-mediated excision[39] before being used in experiments. Mutants were verified by PCR using primers listed in the key resources table. All strains generated in this study are listed in the key resources table.

Mouse studies

Uricase deficient mice

Uox (B6; 129S7-Uox[tm1Bay/J]) mice were resuscitated from frozen embryos by The Jackson Laboratory (strain # 002223). Animal experiments were performed following a protocol approved by the Stanford University Administrative Panel on Laboratory Animal Care. The mouse strain was maintained by heterozygous female (+/-) x homozygous male (-/-) mating. Mice were kept on standard chow (LabDiet Cat. # 5K67) and allopurinol water (100 mg/L) with access to food and water ad libitum in a facility on a 12-hour light/dark cycle with temperature controlled between 20-22°C and humidity between 40-60%. Genotyping was performed using Terra PCR Direct Genotyping Kit (Takara, 639285) following protocol modified from The Jackson Laboratory. For antibiotic treatment, water was supplemented with 0.5 mg/mL vancomycin, 1 mg/mL neomycin, 1 mg/mL metronidazole and 1 mg/mL colistin. Blood sampling was performed from live mice via the facial vein, collecting ~100 μL of blood into tubes containing concentrated sodium EDTA (final ~12 mM) as an anticoagulant and allopurinol (final ~12 μM) to inhibit xanthine oxidase.[23] After centrifugation at 1,500 g for 10 min at 10 °C, plasma was transferred to new tubes. Urine was collected by manually expressing urine from individual mice into sterile tubes. Cecal contents were surgically collected from humanely euthanized animals into sterile tubes. All samples were stored at -80 °C. Uric acid and creatinine were measured by LC-MS, and urea was measured by Urea Assay Kit.

Gnotobiotic mouse experiments

Mouse experiments were performed on male or female gnotobiotic C57BL/6 germ-free mice (8-12 weeks of age) originally obtained from Taconic Biosciences (*Mus musculus*, Tac:B6) maintained in aseptic flexible film isolators (CBC, Madison, WI). Animal experiments were performed following a protocol approved by the Stanford University Administrative Panel on Laboratory Animal Care. Mice were maintained on standard chow (LabDiet Cat. # 5K67) and sterile water with access to food and water ad libitum in a facility on a 12-hour light/dark cycle with temperature controlled between 20-22 °C and humidity between 40-60%. Sterility of germ-free mice was confirmed before each experiment by culturing fecal pellets from each mouse anaerobically in GAM medium for 48 h. For chemically induced hyperuricemia experiments, mice were fed either a casein-fiber refined control chow (TD.210629), a casein-fiber plus 3% oxonic acid chow (TD.210630), or a casein-fiber plus 3% oxonic acid and 3% uric acid chow (TD.210631). Timing of chow administration, colonization, and sampling is outlined in the experimental summaries of the corresponding figures. Bacteria used in mouse experiments were cultured overnight anaerobically at 37 °C in rich medium, mixed in equal volumes as necessary, and administered to individual mice via intragastric gavage. Diets were formulated by Invito (formerly Envigo) and diet compositions are provided in Data S2.

METHOD DETAILS

Reagents used in this study

All chemicals and reagents used in this study were of the highest possible purity and are listed in the key resources table. Uniformly labeled [$^{13}C_5$] uric acid was synthesized by Acanthus Research Inc. (Mississauga, Ontario, Canada). This chemical is available for purchase from Acanthus Research Inc. as catalog # U-10826-01. Due to solubility issues, uric acid or its $^{13}C_5$ isotopolog was made fresh as follows: stock solutions of uric acid were prepared at 125 mM in 1 N NaOH (for screening) or 120 mM in 0.4 N NaOH (for all other experiments), sterile filtered and then diluted appropriately in anaerobic media for uric acid consumption assays.

Bacterial strains and culture conditions

Bacterial strains used in this study were obtained from culture collections as listed in Table S4 and medium formulations are provided in Table S4. All bacteria were cultured at 37 °C in a Coy type B anaerobic chamber using a gas mix containing 5% hydrogen, 10%

carbon dioxide, and 85% nitrogen. An anaerobic gas infuser was used to maintain hydrogen levels of 3.3%. All media and plasticware were pre-reduced in the anaerobic chamber for at least 24 hours before use. *E. coli* for genetic manipulation was cultured under aerobic conditions using LB broth and LB plates, with temperature and antibiotic selection varying depending on the manipulation being done. *E. coli* uric acid consumption was performed under anaerobic conditions using pre-reduced media. For analysis of uric acid consumption under aerobic conditions, *E. coli* or *Enterococcus faecalis* TX2137 were cultured in 1.5 mL volumes in 14 mL round bottom culture tubes at 37 °C with vigorous aeration (300 rpm on an orbital shaker).

Culture conditions for uric acid consumption assays

Bacterial strains used in the library screening, along with their culture media, are listed in Table S4. All strains were stored at -80 °C as anaerobically prepared 20% glycerol stocks, sealed to ensure anoxic conditions for long term storage. All bacteria were cultured in 96-deep well plates anaerobically unless otherwise indicated.

For bacteria library screening, glycerol stocks were first inoculated in rich media without uric acid at 37 °C for 24 h. Cultures were then diluted (10-fold) into medium containing uric acid (5 mM) and continued to incubate for 48 h. The cells were sedimented by centrifugation at 5,000 g for 25 min, 4 °C. Aliquots of supernatants were transferred to 96-well microtiter plates, tightly sealed, and stored at -80 °C prior to sample preparation for LC-MS analysis. Uric acid precipitation may influence our results in our screening assays; therefore we chose a relatively strict threshold of 50% uric acid consumption to identify uric acid consuming bacteria.

For other in vitro culture assays, bacteria were first streaked on GAM or RCM plates, and individual well-isolated colonies were picked to inoculate in liquid medium. *E. coli* was cultured in modified GAM broth unless otherwise indicated. Other strains were cultured in GAM broth. Individual colonies were picked and inoculated in rich media with 2 mM uric acid for 16-18 h and then diluted 50-fold in media with 4 mM uric acid. At designated time points, aliquots of cultures were harvested by centrifugation (5,000 g, room temperature, 5 min). Supernatants were collected and aliquoted into two plates, one that was used for SCFA measurement, and the other that was mixed with NH_4OH (final 10 mM) and used for uric acid measurement. Both plates were stored at -80 °C until analysis by LC-MS.

Stable isotope tracing with $^{13}C_5$ labeled uric acid

For stable isotope tracing, strains were first cultured in rich medium with unlabeled uric acid (2 mM) for 16-18 h before being diluted into medium supplemented with either unlabeled uric acid (4 mM) or uniformly $^{13}C_5$ labeled uric acid (4 mM). At designated times, aliquots were harvested as described above. When cultured without labeled uric acid, isotopologs (e.g., M+2 acetate and M+2 butyrate) were detectable in some of the cultures. We found that this reflected isotope natural abundances resulting from the large amount of short chain fatty acids produced from nutrients (amino acids and carbohydrates) present in the rich medium. Therefore, to correct for natural isotope abundance, we cultured organisms with labeled and unlabeled uric acid. After quantifying SCFA isotopologs, we subtracted concentrations of isotopologs in cultures with unlabeled uric acid from those cultured with labeled uric acid.

Sample preparation for analysis of uric acid, xanthine, and creatinine by liquid chromatography – mass spectrometry (LC-MS)

Uric acid or xanthine was made fresh at 120 mM in 0.4 N NaOH each time. Creatinine was dissolved at 500 mM in LC-MS grade water and stored at -20 °C. The stock solutions were diluted in 10 mM aqueous NH_4OH to serve as a calibration standard for LC-MS assays. To account for matrix effects, the same portion of medium or double charcoal treated human plasma was added to the standard curves for in vitro samples or mouse plasma samples, respectively. Because charcoal treated human serum still has ~100 μM uric acid and ~70 μM creatinine, freshly made $^{13}C_5$-uric acid and creatinine-d5 were used as calibrants for plasma measurements. Calibrants were treated the same as samples during LC-MS preparation.

Culture supernatants, mouse plasma, mouse urine or calibrants were first mixed with internal standard (ISTD) and 10 mM NH_4OH, and then filtered by AcroPrep Omega 3K MWCO filter plates (Pall Corporation, 8033) at 3,000 g for 30 min at room temperature. The flow through was collected and diluted in NH_4OH (final 3 to 5 mM) before subjecting to LC-MS analysis.

For mouse cecal samples containing low amount of uric acid ($\leq$ 5 nmol/mg), 100 ± 10 mg samples were weighed in 2 mL impact resistant screw cap tubes (USA Scientific, 1420-9600) containing ~100 mg glass beads (Sigma, catalog no. G1145) and 150 μL ISTD. Then 750 μL extraction solution (75% acetonitrile/25% methanol) was added and samples were homogenized with a mixer mill (RETSCH MM400) at room temperature, 25/s, for 30 min. The supernatant was collected after centrifugation at 13,000 g for 5 min at room temperature. Supernatants were then diluted 5-fold in LC-MS water and submitted for LC-MS analysis.

For mouse cecal contents containing high amount of uric acid, 50 ± 5 mg cecal contents were weighed in 2 mL impact resistant screw cap tubes (USA Scientific, 1420-9600) containing glass beads (Sigma, catalog no. G1145) and 950 μL 20 mM ammonium hydroxide. Samples were homogenized with a mixer mill (RETSCH MM400) at room temperature, 25/s, for 30 min, and then centrifuged at 13,000 g for 5 min at room temperature. 100 μL of ammonium hydroxide extracted supernatants were mixed with 150 μL ISTD and 750 μL extraction solution (75% acetonitrile/25% methanol), and vortexed for 5 seconds. Then the samples were centrifuged at 13,000 g for 5 min at room temperature. Supernatants were collected and diluted 5-fold in LC-MS water and submitted for LC-MS analysis.

Mouse cecal calibrants were freshly made and serial diluted in 10 mM phosphate buffer, pH 7.5. 100 μL cecal calibrant was mixed with 150 μL ISTD and 750 μL extraction solution (75% acetonitrile/25% methanol), and vortexed for 5 seconds. Samples were then

centrifuged at 13,000 g for 5 min at room temperature. Supernatants were collected and diluted 5-fold in LC-MS water and submitted for LC-MS analysis.

Sample preparation for analysis of short chain fatty acids by LC-MS

Culture supernatants were first mixed with internal standard (ISTD) in a V-bottom, polypropylene 96-well plate, and then extracted by mixing with extraction solution (75% acetonitrile/25% methanol) at 1:3 ratio. The plate was covered with a lid and centrifuged at 5,000 g for 15 min at 4 °C. Supernatant was collected for 3-nitrophenylhydrazine derivatization before subjecting to LC-MS analysis.

3-Nitrophenylhydrazine (NPH) derivatization protocol

This derivatization method targets compounds containing a free carboxylic acid. Extracted samples were diluted in 50% acetonitrile and then mixed with 3-nitrophenylhydrazine (200 mM in 80% acetonitrile) and N-(3-dimethylaminopropyl)-N'-ethylcarbodiimide (120 mM in 6% pyridine) at 2:1:1 ratio. The plate was sealed with a plastic sealing mat (Thermo Fisher Scientific cat. # AB-0566) and incubated at 40 °C, 600 rpm in a thermomixer for 60 min to derivatize the carboxylate containing compounds. The reaction mixture was quenched with 0.02% formic acid in 20% acetonitrile/water before LC-MS analysis.

Quantification of metabolites by liquid chromatography-mass spectrometry (LC-MS)

During this study, two different LC-MS conditions were used (C18 positive underivatized and 3-nitrophenylhydrazine derivatized C18 negative). An overview of the general method is provided here and the specific instrument parameters for the different analytical methods are provided in Table S5. Samples were injected via refrigerated autosampler into mobile phase and chromatographically separated by an Agilent 1290 Infinity II UPLC and detected using an Agilent 6545XT Q-TOF equipped with a dual jet stream electrospray ionization source operating under extended dynamic range (EDR 1700 m/z). MS1 spectra were collected in centroid mode, and peak assignments in samples were made based on comparisons of retention times and accurate masses from authentic standards using MassHunter Quantitative Analysis v.10.0 software from Agilent Technologies. Compounds were quantified from calibration curves constructed with authentic standards using isotope-dilution mass spectrometry with appropriate internal standards (Table S5).

RNA purification for RNA-seq experiment

All cultures were grown at 37 °C under anaerobic conditions. *Clostridium sporogenes* ATCC 15579, *Collinsella aerofaciens* ATCC 25986, and *Lacrimispora saccharolytica* WM1 were streaked from frozen stocks onto blood agar plates. Three individual colonies were selected for each bacterium and were inoculated into separate overnight cultures in Mega medium. The following day, each culture was precultured in Mega medium, and after three hours diluted to an OD of 0.1 into two experimental cultures, one containing standard Mega medium and one with Mega medium containing 5 mM uric acid. Bacteria were allowed to grow until reaching an OD that was commensurate with approximately 50% uric acid degradation as determined by previous experiments. Cell cultures were then combined with two volumes of RNAprotect (Qiagen) in an anaerobic chamber, mixed thoroughly and then allowed to sit for five minutes. Cells were then centrifuged (5,000 g, 4 °C, 10 min) and the supernatant was decanted. Cells were then subjected to lysozyme digestion, Proteinase K digestion and mechanical disruption with a mixer mill (RETSCH MM400) at 4 °C, 25/s, for 30 min. RNA was then purified using RNeasy kit (Qiagen), followed by DNase digestion and second RNA purification step using the RNeasy kit (Qiagen). RNA integrity was determined using a bioanalyzer (Agilent) and RNA-seq was performed by the Roy J. Carver Biotechnology Center at the University of Illinois.

RNA-seq library preparation and data collection

Ribosomal RNA was removed with the Ribo-Zero Bacteria kit (Illumina). The RNA-seq libraries were prepared using a TruSeq Stranded mRNAseq Sample Prep kit with each sample individually ligated with unique adapters (Illumina). The libraries were quantitated by qPCR, pooled, and sequenced on one lane for 101 cycles from one end of the fragments on a NovaSeq 6000 using a NovaSeq SP reagent kit. Fastq files were generated and demultiplexed with the bcl2fastq v2.20 Conversion Software (Illumina) and adaptors were removed from the 3' end of the reads. Read 1 aligns to the antisense strand and read 2 aligns to the sense strand.

RNA-seq data analysis

RNA-seq processing was performed using CLC Genomics Workbench (v.21.0.4). Reads were trimmed using a quality score limit of 0.05 and ambiguous nucleotides (n = 2), and automatic read-through adapter trimming was performed. Next, genomes were downloaded from NCBI in GenBank file format (.gbff) for each of the three bacteria (NCBI assembly accession numbers: GCF_010509075.1, *Collinsella aerofaciens* ATCC 25986; GCF_000144625.1, *Lacrimispora saccharolytica* WM1; GCF_000155085.1, *Clostridium sporogenes* ATCC 15579). Genomes were uploaded into CLC Genomics Workbench and converted to tracks. RNAseq was performed using the genome track as the reference sequence and genes for the gene track. Mapping settings included: Mismatch cost, 2; Insertion cost, 3; Deletion cost, 3; Length fraction, 0.8; Similarity fraction, 0.8; maximum number of hits for a read, 10. Expression settings included: Strand setting, both; Library type setting, bulk; Expression value, TPM. Statistical comparisons were made between organisms cultured with or without uric acid using multi-factorial statistics based on a negative binomial GLM as implemented in CLC Genomics Workbench (v.21.0.4). The expression and CDS tracks were then exported as Excel files and expression and annotation tracks were merged in Excel using the VLOOKUP function based on the chromosome coordinates. For volcano plots, the -Log_{10} False Discovery Rate (FDR) corrected P-value was plotted against the Log_2 fold-change for cultures grown with vs. without uric acid.

RNA purification for RT-qPCR

All cultures were grown at 37 °C under anaerobic conditions. *Escherichia coli* MG1655 was streaked out from frozen stocks onto GAM plates. Individual colonies were selected and were inoculated into separate cultures in GAM modified medium with or without 2 mM uric acid. Three individual cultures were used for each condition. After 16 hours, the overnight cultures were diluted 50-fold in GAM modified medium with or without 4 mM uric acid and continued to incubate at 37 °C. At 24 h, 31 h and 48 h, one aliquot of culture was saved for uric acid LC-MS measurement, and another aliquot of culture was mixed with two volumes of RNAprotect Bacteria Reagent anaerobically to stabilize the RNA. RNA was extracted as described above. The total RNA concentration was measured by Qubit RNA BR Assay Kit. Two micrograms of total RNA were used for ezDNase digestion and then was reverse transcribed to cDNA by SuperScript IV VILO in a 20 μL reaction following manufacturer's guidelines. Q-PCR was performed using PowerUp SYBR Green Master Mix with 4 replicates and an Applied Biosystems QuantStudio™ 5 real-time PCR instrument (ThermoFisher). *E. coli* gDNA concentration was measured using Qubit dsDNA BR Assay Kit. Primer validation was performed using six serial 10-fold dilutions of *E. coli* gDNA, spanning 2 ng/μL to 0.002 pg/μL per reaction. Primer amplification factor (Ep) and efficiency were calculated by ThermoFisher qPCR Efficiency Calculator. Three housekeeping genes (*dnaK*, *fliA* and *rpoH*) were tested and *rpoH* was selected as the reference gene because its Ct was consistent regardless of uric acid addition and was most similar to the Ct of target genes. Relative fold change of the target gene was calculated as follows:

$$Fold\ change\ (normalized) = \frac{(Ep, target)^{\Delta Ct, target}}{(Ep, reference)^{\Delta Ct, reference}} \qquad \text{(Equation 1)}$$

Stable isotope tracing in Uox mouse cecal contents

Fresh cecal contents (∼20 mg) were resuspended in 200 μL 1X M9 salts with uniformly $^{13}C_5$ labeled uric acid (final 4 mM) and Cysteine-Na$_2$S (final 0.025%, each) in 1.5 mL tubes. The samples were incubated in an anaerobic chamber at 37 °C. At designated times, the sample tubes were centrifuged at 20,000 g at room temperature for 2 min anaerobically. Supernatant aliquots were harvested and saved one set directly for short chain fatty acids measurement and another set in ammonium hydroxide (final 10 mM) for uric acid measurement. The rest of the sample were resuspended again and continued to incubate at 37 °C until next time point. Supernatant samples were stored at -80 °C until sample processing and LC-MS analysis for uric acid and short chain fatty acids as described above.

Metagenomic analysis of uric acid genes in cecal contents of Uox mice

Freshly collected cecal contents (∼100 mg) were used for RNA purification by RNeasy PowerFecal Pro Kit (QIAGEN, 78404) and ∼100 mg samples were saved at -80 °C until DNA extraction using QIAamp PowerFecal Pro DNA Kit (QIAGEN, 51804). Following extraction, purified genomic DNA was quantified using a Qubit fluorometer (ThermoFisher). Between 100-500 ng of each sample were taken forward to construct metagenomics sequencing libraries using the Illumina DNA Prep kit, with half-volumes being utilized at each step to minimize cost. Post PCR, libraries were purified using a 0.8x bead clean and were quantified again using the Qubit. Equal masses of each metagenomics library were pooled, and a dual-sided AMPure XP (Beckman Coulter) bead clean was performed on the pooled material to ensure proper size-selection for sequencer loading. Sequencing was performed on the NovaSeq6000 (Illumina) using a PE155 read configuration.

The read pre-processing was done by YAMP (Yet Another Metagenomic Pipeline) from https://github.com/alesssia/YAMP. It included 1) quality trimming/filtering (bbduk.sh adapterFile="adapters" k=23, hdist=1, qtrim=rl, ktrim=r, trimq=10, minlen=60), with adaptors removed with kmer right trimming, kmer size of 23, Hamming distance 1 (allowing one mismatch), quality trimming of both sides of the read, trimming to a Q10 quality score, and removal of reads with length <60 bp; 2) synthetic contaminants removal (bbduk.sh) such as synthetic sequences (PhiX) and sequencing artefacts; 3) Decontamination. Removes external organisms using given genomes - masked version of hg19 at https://zenodo.org/record/1208052#.ZBkj57TMIeM. (bbmap.sh and bbwrap.sh, minid=0.95, maxindel=3, bwr=0.16, bw=12, minhits=2), with minimum alignment identity 0.95, longest indel 3, restrict alignment band to 0.16 of read length, alignment bandwidth 12, and Hamming distance 2 (allowing two mismatches). All pre-processing was carried out using BBtools v. 38.87 for short reads.

Pre-processed reads were uploaded to KBase as paired end libraries and merged into two separate read libraries, one for Uox$^{+/-}$ mice (n = 4 input libraries) and one for Uox$^{-/-}$ mice (n = 8 input libraries). The two merged libraries were then separately assembled using MEGAHIT (v.1.2.9) with the meta-large parameter and minimum contig length of 2,000 bp. The Uox$^{+/-}$ and Uox$^{-/-}$ assemblies consisting of 400,154 and 359,786 contigs, respectively were exported and used to create nucleotide BLAST databases using Geneious Prime (v.11.1.5). These databases were searched for homologs of the *C. sporogenes* YgeX protein sequence (GenBank EDU35956.1) using tBLASTn. Contigs containing BLAST hits with ≥ 50% amino acid identity were filtered by contig length >10,000 bp and redundancy filtered at 95% average nucleotide identity, then uploaded into KBase and annotated using Prokka (v.1.14.5). Finally, GenBank files were exported and eight uric acid gene clusters were identified by MultiGeneBlast searches with the *C. sporogenes* gene cluster as a query. Metagenomic read mapping was performed using CLC Genomics Workbench (v.21.0.4). Reads from Uox$^{+/-}$ mice (n = 4 input libraries) or Uox$^{-/-}$ (n = 8 input libraries) were individually mapped to the eight uric acid gene clusters with a length fraction of 0.8 and similarity fraction of 0.98. Data were converted to reads per kilobase per million reads mapped using the number of reads mapped, the gene cluster length, and the number of reads per input library.

Total RNA was isolated from fresh cecal contents (∼100 mg) by RNeasy PowerFecal Pro Kit (QIAGEN, 78404) and then was reverse transcribed to cDNA by SuperScript IV VILO after ezDNase digestion. Q-PCR was performed using PowerUp SYBR Green Master Mix with 4 technical replicates using an Applied Biosystems QuantStudio™ 5 real-time PCR instrument (ThermoFisher). The genomic DNA and total RNA concentration was measured by Qubit dsDNA BR Assay Kit and by Qubit RNA BR Assay Kit, respectively. A standard curve of each primer set (key resources table) was performed using cecal genomic DNA and based on this result, final 1 ng/μL of genomic DNA or cDNA was used in the qPCR reaction. The relative amount of genomic DNA or cDNA was calculated based on the standard curve. The normalized gene expression was calculated using relative amount of cDNA divided by relative amount of genomic DNA.

Impact of antibiotic treatment on risk for Gout diagnosis

We conducted a retrospective new user cohort study[41] using electronic health records (EHR) collected during from the Stanford Health Care system between 2015 and 2019. EHR were mapped to the Observational Medical Outcomes Partnership (OMOP) Common Data Model (CDM) version 5.3 such that standardized vocabularies like the RxNORM and International Classification for Diseases (ICD) could be used to define patients and their conditions (Table S3). Patients between 18 and 90 years old were included in the cohort if they were prescribed at least 5 days of oral Bactrim and Clindamycin and if they did not receive antibiotics in the preceding 3 months. Primary outcome was gout diagnosis up to 5 years after antibiotic treatment (see Table S3 for detailed definitions). The study only included de-identified data and qualified for exempt status by the Institutional Review Board of Stanford University.

Propensity score model

We created a multivariable logistic regression model to calculate the probability of patients receiving Clindamycin or Bactrim. The propensity score (PS) regression model controlled for the following pre-exposure confounders: age, sex, race/ethnicity, Charlson comorbidities,[42] diagnostic, procedure and medication codes, and number of encounters observed in the 90 days before antibiotics initiation.

The propensity score provides a composite score of the baseline confounders such that when PS is balanced (within a caliper of 0.25) between the Bactrim and Clindamycin arms, their baseline confounders would also become balanced.[43] We used high dimensional propensity scores (hdPS).[44] First, hdPS covariates were generated from ICD, CPT and RxNORM codes. A model of the hdPS covariates is fitted using a logistic regression with LASSO regularization that penalizes low weight covariates down to zero weights such that the resulting parsimonious model has equivalent predictive performance without overfitting too many covariates in a high dimensional setting.[45,46] The LASSO hyperparameter is tuned using 5-fold cross-validation and the 1-standard error rule.[47] A two-sided P-value of 0.05 was considered statistically significant. Analyses were performed using R version 4.05 on the Atropos Health platform.[48]

Metagenomic analysis of uric acid gene cluster abundances in the FARMM study

To create a new uric acid detection rule for the metabolic gene cluster (MGC) prediction software gutSMASH,[28] we focused our search on six individual marker genes from *Clostridium sporogenes* (i.e. *ygeX*, *hyuA*, *ygfK*, *ssnA*, *ygeY* and *xdhAC*). Homologs of these marker genes were gathered from 2,357 protein sequences of the Microbial Reference Genomes collection of the Human Microbiome Project (HMP). Percentage amino acid identity cutoffs were pre-determined based on individual BLASTp searches of *C. sporogenes* sequences against an in-house strain library of experimentally verified uric-acid-consuming strains. For profile hidden Markov model (pHMM) construction, we included homologs that share at least 80% sequence coverage and meet the resulting amino acid identity cutoffs of 50%, 36%, 41%, 33%, 53% and 46%, respectively. The retrieved amino acid sequences were aligned with MUSCLE v.3.8.1551[49] and profiles were built using hmmbuild (HMMER v.3.3.2, December 2021; http://hmmer.org/). Known uric acid cluster homologs were manually searched using hmmsearch (HMMER v.3.3.2, December 2021; http://hmmer.org/) to determine a bit score cutoff for true and false positive hit delineation. The resulting uric acid MGC detection rule was applied using gutSMASH on a collection of 4,254 human microbiome genomes as described by Pascal Andreu et al.[28] Resulting uric acid predicted MGCs were used as input for the gene cluster abundance assessment tool BiG-MAP.[29] With the use of the BiG-MAP.family module, we grouped the 782 MGCs into 107 gene cluster families (GCFs). Next, we mapped metagenomic reads of 474 individuals reported by Tanes et al.[26] onto 107 representative MGCs with the use of BiG-MAP.map. Resulting RPKM counts were normalized using cumulative sum scaling (CSS) from the R Bioconductor package MetagenomeSeq[50] to correct for differences in sequencing depth. Linear regression was applied to adjust for possible covariates such as age and body mass index (BMI). The residuals from the linear regression model were used to perform an ANOVA and pairwise comparisons P-value for the pathway abundance. The results are visualized using the R packages ComplexHeatmap[51] and ggpubr of ggplot2.[52]

QUANTIFICATION AND STATISTICAL ANALYSIS

All statistical analyses and definitions of sample sizes are provided in the figure legends. At least three biological replicates were tested unless otherwise specified. Error bars in bar graphs or line graphs represent standard deviation of the data.

Supplemental figures

A **Carbohydrate-limited conditions**
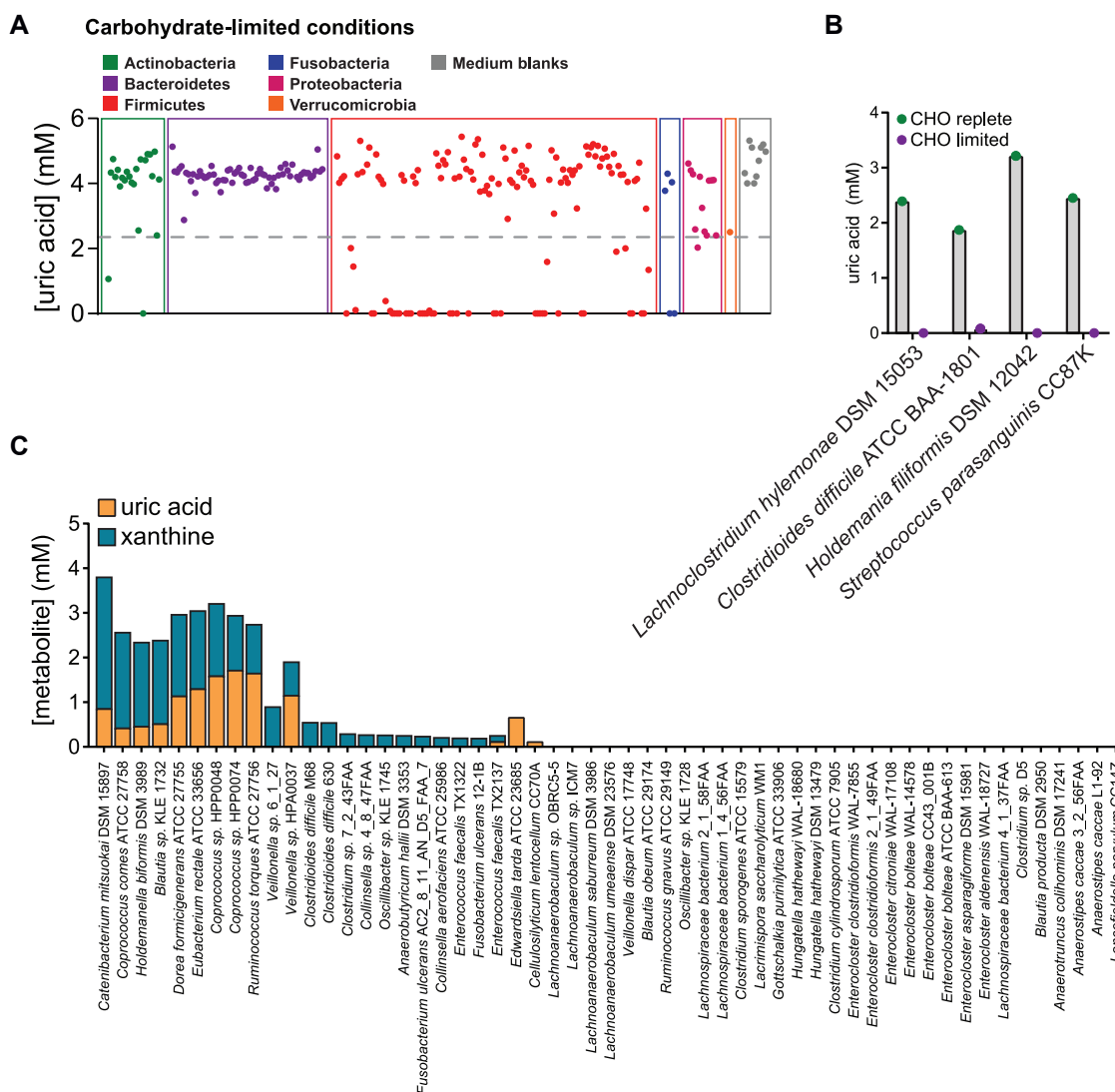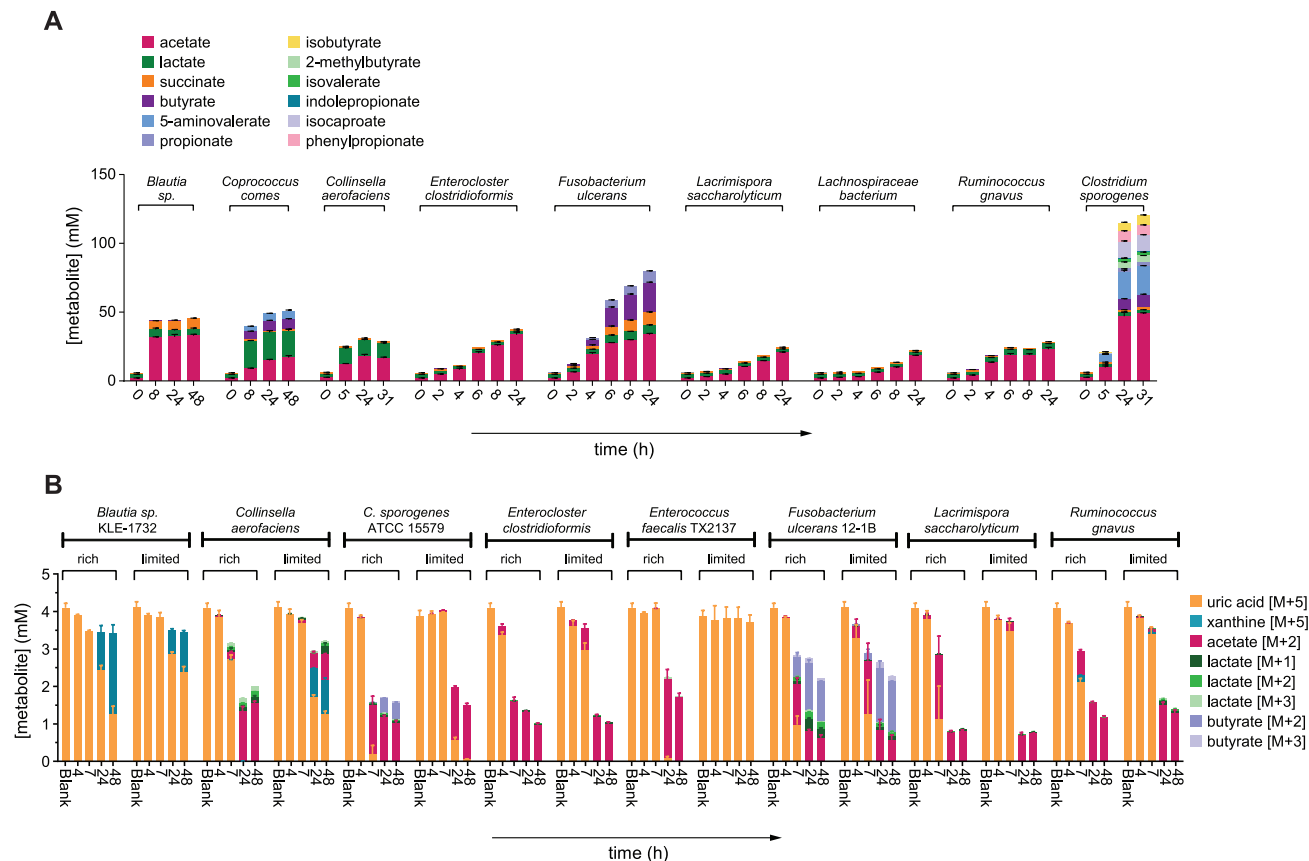
B

C

Figure S1. Influence of carbohydrates on uric acid metabolism and detection of xanthine in cultures, related to Figure 1

(A) Bacteria were cultured for 48 h in rich medium with limited carbohydrates and uric acid was quantified by LC-MS. Each dot represents a single bacterial strain and organisms are grouped by phylum.

(B) Bacteria that degrade uric acid in carbohydrate limited medium, but not in carbohydrate supplemented medium. Strains are shown that consumed <50% uric acid in carbohydrate supplemented medium and consumed >50% uric acid when carbohydrates were limited. For (A) and (B), data represent the results from a single experiment.

(C) Xanthine and uric acid were quantified in the supernatant of both screening experiments after 48 h by LC-MS. Only those strains that consumed ≥50% uric acid are shown. Data represent the results from a single experiment.

Figure S2. Short chain fatty acid production in rich media and influence of nutrient availability on uric acid metabolism, related to Figure 2

(A) Bacteria were cultured in rich medium supplemented with unlabeled uric acid and short chain fatty acids were quantified by LC-MS at the indicated time points.

(B) Uric-acid-consuming strains were cultured either in rich medium (GAM) or in more limited medium composed of M9 salts, vitamin solution, yeast extract, and tryptone. Media were supplemented with either labeled or unlabeled uric acid and metabolites were quantified by LC-MS at the indicated time points. For (A) and (B), strains include: *Blautia sp.* KLE 1732, *Coprococcus comes* ATCC 27758, *Collinsella aerofaciens* ATCC 25986, *Enterocloster clostridioformis* WAL-7855, *Enterococcus faecalis* TX2137, *Fusobacterium ulcerans* 12-1B, *Lacrimispora saccharolytica* WM1, Lachnospiraceae bacterium 1_4_56FAA, *Ruminococcus gnavus* ATCC 29149, and *Clostridium sporogenes* ATCC 15579. Data represent the mean ± SDs of n = 3 biological replicates.
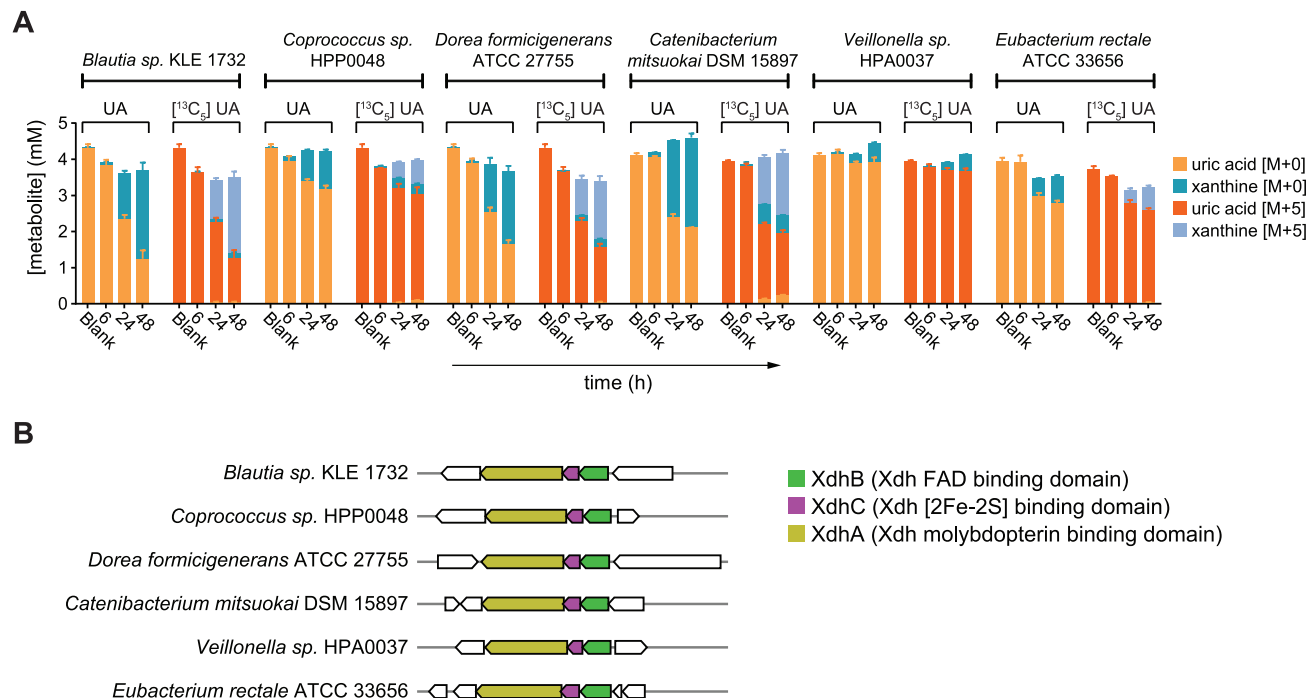
A

B

Figure S3. Stable isotope tracing in uric-acid-consuming strains that do not encode the uric acid gene cluster, related to Figure 5

(A) Bacteria were cultured in chopped meat medium supplemented either with labeled or unlabeled uric acid and metabolites were quantified by LC-MS at the indicated time points. Data represent the mean ± SDs of n = 3 biological replicates.

(B) Analysis of the genome sequences for these xanthine consuming bacteria revealed a conserved gene cluster encoding xanthine dehydrogenase.
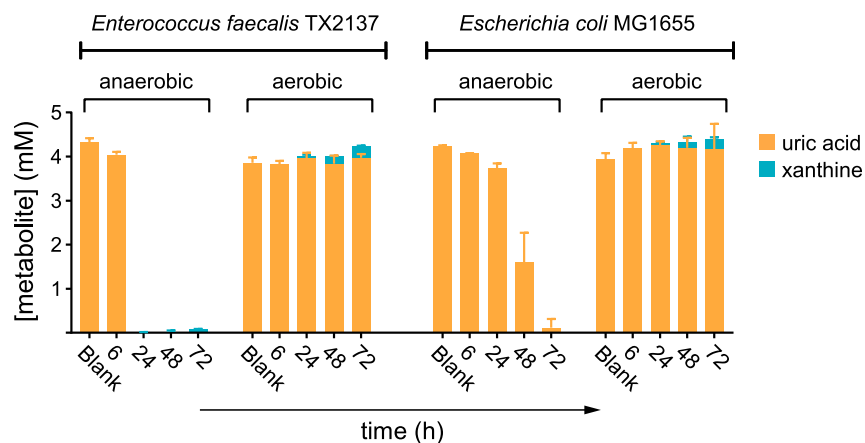
Figure S4. *Enterococcus faecalis* and *Escherichia coli* consume uric acid during anaerobic, but not aerobic growth, related to Figure 6
Enterococcus faecalis TX2137 and *E. coli* MG1655 were cultured in rich medium, either in an anaerobic chamber or aerobically with vigorous aeration. Culture medium was supplemented with unlabeled uric acid, and uric acid and xanthine were quantified at specified time points by LC-MS. Data represent the mean ± SDs of n = 3 biological replicates.
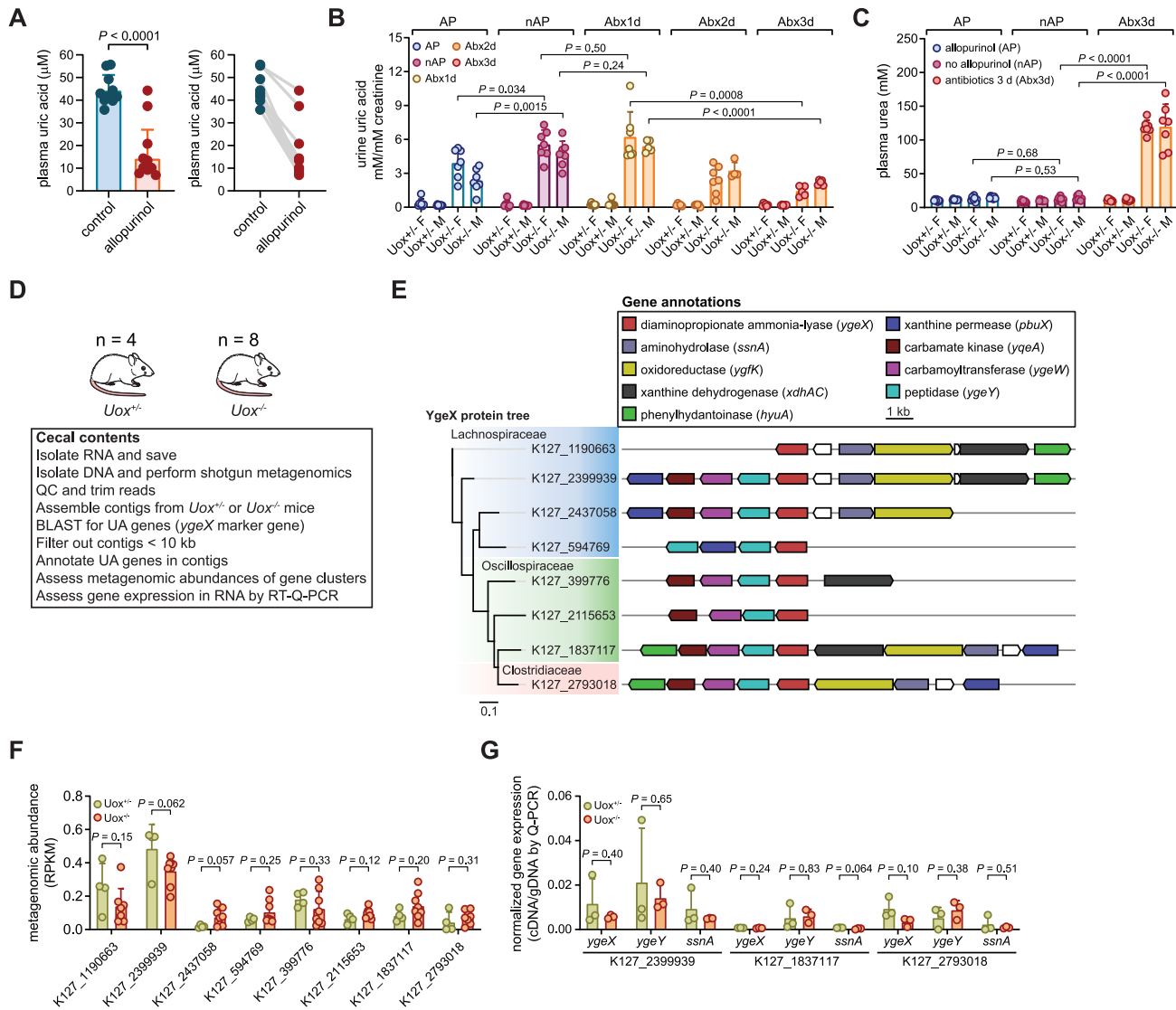
Figure S5. Studies in conventional and uricase-deficient mice, related to Figure 7

(A) Conventional Swiss Webster mice were bled from the facial vein and blood was directly collected into tubes containing either EDTA (control) or EDTA with allopurinol. Uric acid in the plasma was then quantified by LC-MS. The right panel shows individual mice connected by gray lines.

(B) Urine uric acid levels normalized to creatinine in male and female $Uox^{+/-}$ or $Uox^{-/-}$ mice.

(C) Plasma urea levels in male and female $Uox^{+/-}$ or $Uox^{-/-}$ mice. AP, allopurinol in drinking water; nAP, no allopurinol in drinking water; Abx1d, antibiotic treatment for 1 day; Abx2d, antibiotic treatment for 2 days; Abx3d, antibiotic treatment for 3 days.

(D) Overview of approach to analyze uric acid genes in cecal contents of Uox mice.

(E) Gene clusters identified within assembled contigs from $Uox^{+/-}$ or $Uox^{-/-}$ mice.

(F) Metagenomic abundance of gene clusters in $Uox^{+/-}$ or $Uox^{-/-}$ mice.

(G) Gene expression in cecal contents of $Uox^{+/-}$ or $Uox^{-/-}$ mice assessed by RT-qPCR. For (A), data represent the mean ± SDs from n = 10 mice. For (B) and (C), data represent mean ± SDs from n = 7–8 mice per group. For (F), data represent mean ± SDs from n = 4 ($Uox^{+/-}$) or n = 8 (Uox^{-ox}) mice. For (G), data represent mean ± SDs from n = 3 mice per group. p values are from two-tailed unpaired Student's t tests.
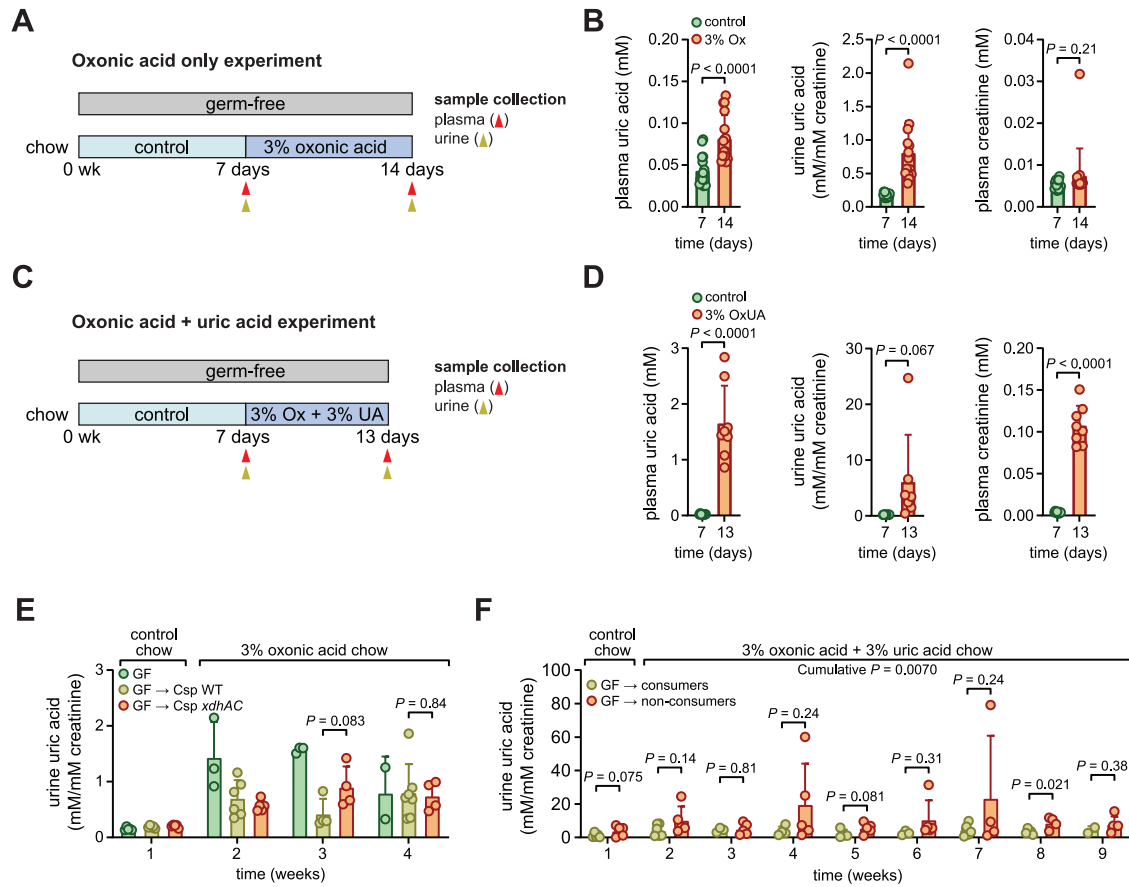
Figure S6. Studies in gnotobiotic mice with chemically induced hyperuricemia, related to Figure 7

(A) 3% oxonic-acid-only model. Germ-free C57Bl/6 Tac mice were fed an isocaloric control chow and then switched to a chow supplemented with 3% oxonic acid.

(B) Uric acid and creatinine were measured at the indicated time points in plasma and urine using LC-MS.

(C) 3% oxonic acid with 3% uric acid model. Germ-free C57Bl/6 Tac mice were fed an isocaloric control chow and then switched to a chow supplemented with 3% oxonic acid and 3% uric acid. Mice met humane endpoint after 5–6 days on OxUA chow and were euthanized.

(D) Uric acid and creatinine were measured at the indicated time points in plasma and urine using LC-MS. For (A) and (C), timing of sample collection is indicated with gold (urine) and red (plasma) arrows. Ox, oxonic acid; UA, uric acid.

(E) Urine uric acid levels normalized to creatinine in mice fed an oxonic-acid-only chow and maintained either germ-free or colonized with WT or *xdhAC* mutant *C. sporogenes*.

(F) Urine uric acid levels normalized to creatinine in mice fed an oxonic acid + uric acid chow and colonized a uric acid consumer community or a phylogenetically matched non-consumer community. For (B), data represent mean ± SDs from n = 15 mice. For (D), data represent the mean ± SDs from n = 8 mice. For (E), data represent mean ± SDs from n = 5–7 mice per group. For (F), data represent mean ± SDs from n = 6 mice per group. p values are from two-tailed unpaired Student's t tests.

A FARMM Study

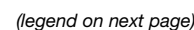**B**

C Abundance

(legend on next page)

Figure S7. Uric acid gene cluster abundances in study subjects in the FARMM study, related to Figure 7

Data were re-analyzed from the Food and Resulting Microbial Metabolites (FARMM) study exploring the role of diet in microbiome metabolite recovery after disruption with antibiotics and polyethylene glycol.

(A) Fecal uric acid levels for each study subject are plotted as means with confidence intervals representing SEMs. Gray region indicates time in which antibiotics and PEG were administered to study participants. AUC, area under the curve.

(B) Uric acid gene cluster abundances in study subjects before, during, and after microbiota depletion. Metagenomic data from study subjects were mapped to uric acid gene cluster families using gutSMASH and BiG-MAP. Resulting reads per kilobase per million reads mapped (RPKM) were normalized by cumulative sum scaling and are plotted as mean ± SDs.

(C) Metagenomic data from study subjects were mapped to uric acid gene cluster families using gutSMASH and BiG-MAP. Heatmap showing abundance of 107 uric acid gene cluster families within fecal metagenomic samples from study subjects before, during, and after microbiota depletion. Yellow boxes indicate gene cluster abundances that are lower for EEN study subjects compared with omnivore and vegan subjects.